Direct measurement of N_2O_5 heterogeneous uptake coefficients on ambient aerosols via an aerosol flow tube system: design, characterization and performance

Xiaorui Chen[1,a], Haichao Wang[3,4*], Tianyu Zhai[1], Chunmeng Li[1], Keding Lu[1,2*]

[1]State Key Joint Laboratory of Environmental Simulation and Pollution Control, College of Environmental Sciences and Engineering, Peking University, Beijing, China.

[2]The State Environmental Protection Key Laboratory of Atmospheric Ozone Pollution Control, College of Environmental Sciences and Engineering, Peking University, Beijing, China

[3]School of Atmospheric Sciences, Sun Yat-sen University, Zhuhai, 519082, China

[4]Guangdong Provincial Observation and Research Station for Climate Environment and Air Quality Change in the Pearl River Estuary, Key Laboratory of Tropical Atmosphere-Ocean System, Ministry of Education, Southern Marine Science and Engineering Guangdong Laboratory (Zhuhai), Zhuhai, 519082, China

[a]now at: Department of Civil and Environmental Engineering, The Hong Kong Polytechnic University, Hong Kong, China

Correspondence to: Haichao Wang (wanghch27@mail.sysu.edu.cn), Keding Lu (k.lu@pku.edu.cn)

Abstract. An improved aerosol flow tube system coupled with detailed box model was developed to measure N_2O_5 heterogeneous uptake coefficients ($\gamma(N_2O_5)$) on ambient aerosols directly. This system features sequential measurements of N_2O_5 concentration at the both entrance and exit of the flow tube to ensure an accurate retrieval of N_2O_5 loss in the flow tube. Simulation and laboratory tests demonstrate that this flow tube system is able to overcome the interference from side reactions led by varying reactants (e.g., NO_2, O_3 and NO) and improve the robustness of results with the assistance of box model method. Factors related to $\gamma(N_2O_5)$ derivation were extensively characterized, including particle transmission efficiency, mean residence time in the flow tube and wall loss coefficient of N_2O_5, for normal operating

condition. The measured $\gamma(N_2O_5)$ on $(NH_4)_2SO_4$ model aerosols were in good agreement with literature values over a range of relative humidity (RH). The detection limit of $\gamma(N_2O_5)$ was estimated to be 0.0016 at low aerosol surface concentration (Sa) condition of 200 μm^2 cm^{-3}. Given the instrument uncertainties and potential fluctuation of air mass between successive sampling modes, we estimate the overall uncertainty of $\gamma(N_2O_5)$ that ranges from 16 to 43% for different ambient conditions. This flow tube system was then successfully deployed for field observations at an urban site of Beijing influenced by anthropogenic emissions. The performance in field observation demonstrates that the current setup of this system is capable of obtaining robust $\gamma(N_2O_5)$ amid the switch of air mass.

1 Introduction

Dinitrogen pentoxide (N_2O_5), forming from the reaction of nitrogen dioxide (NO_2) and nitrate radical (NO_3), acts as an important reservoir of atmospheric nitrogen. The N_2O_5 can undergo either thermal dissociation (back to NO_2 and NO_3; photolysis of NO_3 also generate NO_2) to release NO_2 or hydrolysis (both homogeneous and heterogeneous) to remove nitrogen oxides from the atmosphere (Brown and Stutz, 2012;Chang et al., 2011). Among the budgets of N_2O_5, the uptake on aerosol particles is a highly efficient pathway to be responsible for production of nitrate aerosol in some regions (Fu et al., 2020;Wang et al., 2019;Wang et al., 2017c;Baasandorj et al., 2017;McDuffie et al., 2019;Prabhakar et al., 2017;Wang et al., 2018a;Chen et al., 2020) and promote activation of chlorine via $ClNO_2$ formation (Bertram and Thornton, 2009a;Osthoff et al., 2008;Tham et al., 2018;Thornton et al., 2010;Wang et al., 2017f;Riedel et al., 2012a;Riedel et al., 2013;Gaston and Thornton, 2016;Mitroo et al., 2019). The N_2O_5 uptake coefficient ($\gamma(N_2O_5)$) is critical in determining the uptake reaction rate of N_2O_5 on aerosol in addition to aerosol surface area (Sa). It represents the fraction of collisions between gaseous N_2O_5 molecules and particle surfaces that resulted in a loss of N_2O_5. Model simulation showed the variations in $\gamma(N_2O_5)$ can significantly influence the fate of NOx, O_3 and OH radical in a regional (Li et al., 2016;Sarwar et al., 2012;Lowe et al., 2015) and global scale (Dentener and Crutzen, 1993;Evans and Jacob, 2005;Macintyre and Evans, 2010;Murray

et al., 2021). However, ambient data of direct observation on $\gamma(N_2O_5)$ is still scarce. It is thereby necessary to develop an accurate equipment or method to quantify this parameter on ambient aerosols.

Extensive laboratory experiments have been conducted to derive the values of $\gamma(N_2O_5)$ on aerosols and understand the mechanism of N_2O_5 uptake by various methods, including aerosol flow reactor (Kane et al., 2001;Mozurkewich and Calvert, 1988;Hu and Abbatt, 1997;Thornton and Abbatt, 2005;Thornton et al., 2003;Tang et al., 2014;Bertram and Thornton, 2009a;Cosman et al., 2008;Escoreia et al., 2010;Gaston et al., 2014;Folkers et al., 2003), droplet train reactor (Van Doren et al., 1990;Schweitzer et al., 1998), Knudsen flow reactor (Karagulian et al., 2006) and smog chamber (Wahner et al., 1998;Wu et al., 2020). The $\gamma(N_2O_5)$ was found to be highly variable and dependent on particle chemical composition, acidity, size, phase state and the presence of organic coating using these laboratory methods under controllable conditions (Badger et al., 2006;Bertram et al., 2011;Fried et al., 1994;Griffiths et al., 2009;Gross et al., 2009;Hallquist et al., 2000;McNeill et al., 2006;Mentel et al., 1999;Riemer et al., 2003;Gaston and Thornton, 2016;Escoreia et al., 2010;Gaston et al., 2014;Thornton et al., 2003). While laboratory results have contributed to recognize the mechanism of N_2O_5 uptake and develop $\gamma(N_2O_5)$ parameterizations (Anttila et al., 2006;Bertram and Thornton, 2009b;Davis et al., 2008;Griffiths et al., 2009;Riemer et al., 2009), issues might emerge when quantitatively extended to ambient conditions due to the discrepancy between laboratory conditions and real air mass. For example, much higher reactant and particle concentration usually used in laboratory experiments might induce surface saturation or secondary reactions in a short time period, which lead to the bias of reaction rate used in ambient conditions (Thornton et al., 2003). In addition, the physicochemical properties of ambient aerosol are much more complicated that the model aerosol used in laboratory studies, which led to the laboratory results on model aerosols are difficult to accurately represent what happens on the atmospheric aerosols (Royer et al., 2021;Mitroo et al., 2019).

There have been several methods implemented for field campaigns to indirectly derive $\gamma(N_2O_5)$, simply based on observation of ambient NO_3, N_2O_5, NO_2, O_3, $ClNO_2$, pNO_3^- and

other auxiliary parameters without special equipment to capture the decay of N_2O_5 like laboratory ways. These include (1) the linear fit between N_2O_5 (NO_3) lifetime and the product of NO_2 and Sa concentration according to steady state equations (Brown et al., 2002;Brown et al., 2009;Brown et al., 2006;Platt et al., 1984;Wang et al., 2017b;Wang et al., 2017d;Tham et al., 2016;Wang et al., 2017f;Brown et al., 2016), (2) the analysis of production rates of products (pNO_3^- and $ClNO_2$) resulting from N_2O_5 uptake under a stable condition (Mielke et al., 2013;Phillips et al., 2016;Wang et al., 2018b) and (3) box model simulations with an iterative approach to reproduce the evolutions of NO_3-N_2O_5 chemistry within each separate air mass after sunset (McDuffie et al., 2018;Wagner et al., 2013;Wang et al., 2020a;Yun et al., 2018). All these methods contain some specific assumptions and are only applicable in a few special cases.

To directly determine the $\gamma(N_2O_5)$ on ambient aerosols, Bertram et al. (2009a) firstly design an entrained aerosol flow reactor to adapt for low atmospheric Sa concentration with easy operation. By switching between filtered and bypass sampling mode, the N_2O_5 concentration at the exit of flow tube can be measured in the presence and absence of aerosols, respectively. The pseudo-first-order rate coefficients for N_2O_5 loss on aerosols is thereby derived from the ratio of measured N_2O_5 concentration in these two modes within a duty cycle according to Eq. 1:

$$k_{aerosols} = -\frac{1}{\Delta t}\ln\frac{[N_2O_5]_{\Delta t}^{w/particles}}{[N_2O_5]_{\Delta t}^{wo/particles}} \quad \text{Eq. 1}$$

where the Δt is the mean residence time of the flow tube, and the $[N_2O_5]_{\Delta t}^{wo/particles}$ and $[N_2O_5]_{\Delta t}^{w/particles}$ are the measured N_2O_5 concentration at the exit of flow tube in filtered and bypass mode, respectively. Assuming the gas-phase diffusion effect is negligible for atmospheric particles and low reaction probability (γ<0.1) (Fuchs and Sutugin, 1970), $\gamma(N_2O_5)$ can then be calculated from Eq. 2:

$$\gamma(N_2O_5) = \frac{4 \times k_{aerosols}}{c \times S_a} \quad \text{Eq. 2}$$

This method was deployed to measure $\gamma(N_2O_5)$ on ambient particles during two field campaigns (Bertram et al., 2009b;Riedel et al., 2012b) and on aerosols generated in the laboratory (Ahern et al., 2018). While values of $\gamma(N_2O_5)$ were determined to be robust in laboratory experiments, most of data would be dropped under ambient conditions due to the variations of wall loss coefficients (dominated by RH), fresh NO emission, N_2O_5 regeneration and flow pattern inside the flow tube. Based on the above measurement system, Wang et al. (2018c) added NOx, O_3 and Sa measurement on the exit of flow tube and introduce an iterative box model to minimize the potential influences from changing air mass and non-linear response of interference reactions. With the assumption of the equilibrium between NO_3 and N_2O_5, the box model runs backward and forward iteratively to obtain the N_2O_5 loss rate constant in the absence ($k_{het}^{wo/particles}$) and presence ($k_{het}^{w/particles}$) of aerosols respectively. The difference between these two parameters can finally derived the $\gamma(N_2O_5)$ according to Eq. 3, assuming the wall loss effect stays consistent.

$$\gamma(N_2O_5) = \frac{4(k_{het}^{w/particles} - k_{het}^{wo/particles})}{c \times S_a} \quad \text{Eq. 3}$$

This iterative approach was demonstrated to be able to buffer against certain fluctuations of air mass and measure $\gamma(N_2O_5)$ in the polluted atmosphere (Yu et al., 2020b).

Until now, only few direct measurements of $\gamma(N_2O_5)$ on ambient aerosols have been conducted during field campaigns (Bertram et al., 2009b;Riedel et al., 2012b;Yu et al., 2020a). Even though combining with dataset from indirect approaches (e.g. steady state approximations), it is still challenging to characterize the temporal and spatial distributions of $\gamma(N_2O_5)$ on ambient aerosols. To better investigate the reactive uptake of N_2O_5 on aerosols in different environments, we develop an aerosol flow tube system with newly designed gas circuit and data acquisition procedures to quantify $\gamma(N_2O_5)$ on ambient aerosols. In the following sections, the setup of this system and laboratory characterizations for each part are described in details. Procedures of acquiring and processing data are compared to previous methods and discussed with potential uncertainties. Laboratory tests on model aerosols and field observations are presented to demonstrate its performance under varying ambient

conditions.

2 The aerosol flow tube system

A schematic of the aerosol flow tube system is shown in Figure 1. The ambient air enters the system from the sampling manifold, mixes with gaseous N_2O_5 source in a Y-tee and flows to aerosol flow tube and detection instruments, as indicated by arrows in the figure. The design of sampling module and aerosol flow tube in this work follows to previous work for measuring $\gamma(N_2O_5)$ on ambient aerosols (e.g. Bertram et al., 2009). The major improvement of this system from previous work are continuous monitor of NOx and O_3 concentration before the inlet of flow tube (after sampling air mixing with N_2O_5 source) and the sequential measurements of N_2O_5 concentration both at the inlet and the exit of flow tube within a duty cycle. To achieve the programmed cyclic measurement of these key parameters, we adopted a new design of Y-tee with a static mixer inside and cyclic measurement setup. Constraints of these parameters during the data processing can improve the measurement accuracy (see also the discussion in section 3.2).

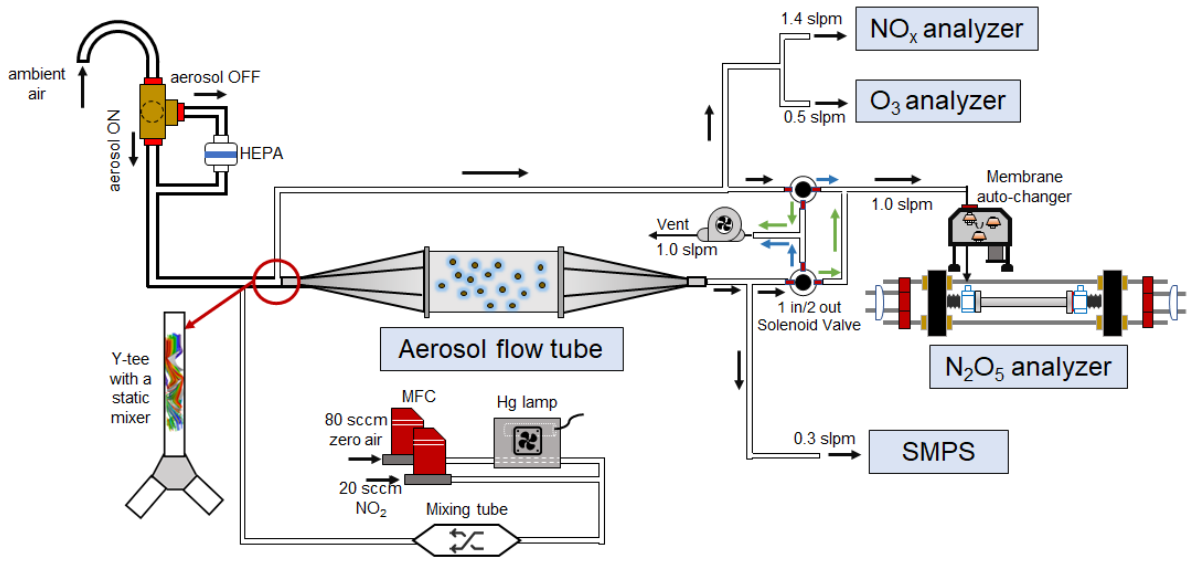

Figure 1. Overall schematic of aerosol flow tube system. The arrows alongside the tube show the flow directions. The black arrows indicate the flow directions consistent during the measurements, green arrows indicate the flow directions active in measuring the exit N_2O_5 and blue arrows indicate the flow directions active in measuring the inlet N_2O_5.

2.1 Sampling manifold

The sampling tube is made of a 50 cm long and half inch outside diameter (OD) aluminum tubing, with a curve tip (10 cm radius of curvature) turning the inlet straight down in order to avoid precipitation. The ambient air is then pass through a three-way solenoid ball valve, which is controlled by a time relay to either allow the air to flow directly into a following Y-tee (filter bypass mode) or divert to a HEPA (high efficiency particulate air filter, Whatman) to remove particles (filter inline mode). We choose a stainless-steel ball valve with the same OD as the sampling tube to minimize the particle loss in filter bypass mode. The HEPA can retain particles at a high efficiency (>99.9%) with low pressure drop and RH difference between filter inline and bypass mode.

2.2 Gaseous N_2O_5 generation

A home-made temperature-controlled gas generator is used to generate gaseous N_2O_5 in-situ via the reaction of O_3 with NO_2 (R1) and the subsequent reaction of produced NO_3 with NO_2 (R2).

$$NO_2 + O_3 \rightarrow NO_3 + O_2 \qquad \text{R1}$$

$$NO_2 + NO_3 + M \leftrightarrow N_2O_5 + M \qquad \text{R2}$$

NO_2 is delivered from a compressed gas cylinder (20 ppmv in N_2 diluent gas, Jinghao Corp.). O_3 is generated from the photolysis of O_2 in compressed ultra-pure synthetic zero air at 254 nm, using a commercial mercury lamp (UVP, the USA) fixed inside the generator. The produced O_3 are then mixed with NO_2 in a small darkened Teflon reaction tube for about 2 min under the temperature of 15 ℃, stabilized by a Peltier cooler controlled by a proportion integration differentiation algorithm. A PFA tube with polyethylene foam was used to transmit the synthesized N_2O_5 to sampling stream and minimize the influence of ambient temperature variation on N_2O_5 level. The flow rate of NO_2 (20 sccm) and zero air (80 sccm) are controlled by mass flow controller separately at a total of 100 sccm. By changing the flow rate ratio between NO_2 and zero air, the generator can produce N_2O_5 concentration varying from 1 ppbv to 6 ppbv (after dilution in zero air at sampling flow rate of 4.5 slpm). Under the typical

measurement condition, an excess of NO_2 concentration is applied to shift the equilibrium towards N_2O_5 production (R2) and suppress the NO_3 concentration to less than 30 pptv, which is expected to decrease the uncertainty of varying NO_3 reactivity (NO, VOCs and heterogeneous loss). The resulted initial N_2O_5 concentration was 4.0 ppbv at the inlet of aerosol flow tube, together with around 50 ppbv of NO_2 and 15 ppbv of O_3. A stability test on N_2O_5 source showed the variation was within 1% for a 24-h continuous operation, with ambient temperature ranging from 0 to 15 ℃.

2.3 Aerosol flow tube

Air flow enters and exits the flow tube via two identical conical diffuser caps at a diffuser angle of 45°. A 35cm×14 cm inner diameter (ID) cylindrical tube is mounted in the middle of two caps, flanged with screws and nitrile rubber O-rings. All sections of this aerosol flow tube are made of stainless-steel with electro-polished and FEP-coated inside. The exterior of the flow tube is insulated with aluminum coated polyethylene foam 3 cm thick to minimize thermal eddies fluctuation of ambient temperature. The mechanic design of this flow tube follows that used in Bertram et al. (2009), with different length and diffuser angles particularly designed for our typical flow rate. Under the typical flow rate of 2.1 SLPM in the flow tube, the axial velocity in the cylindrical tube section is 0.23 $cm \cdot s^{-1}$ which produces a Reynolds numbers (*Re*) of 22, well below the threshold of laminar flow (*Re*<2100).

In front of the flow tube, the synthesized N_2O_5 source is introduced perpendicular to ambient air sampling stream via a regular stainless-steel tee and then the mixture enters a stainless-steel Y-tee for further mixing. The inner surface of both regular tee and Y-tee is electro-polished and coated with SilcoNert 2000 (Silotek Corp.), a technique commonly applied in semiconductor industry, to maintain the transmission efficiency of particles and minimize the loss of N_2O_5 in the meantime. A 10 cm long stainless-steel static mixer is mounted inside the Y-tee in order to swirl the flow and thus facilitate the mixing between sampling stream and N_2O_5 source in a relatively short distance. The presence of static mixer at the inlet also help to improve the flow expansion performance after entering the flow tube by minimizing flow recirculating towards the wall, which decreases the wall loss of N_2O_5 and

particles (Huang et al., 2017). After passing through the static mixer, the mixture of ambient air and N_2O_5 source is split into two flows at the same flow rate, one of which straightly enters the aerosol flow tube and the other one is diverted to measurements of NOx, O_3 and N_2O_5. We measured the concentrations of NOx, O_3, N_2O_5 and Sa at the both exits of Y-tee under typical flow rate for three repeated experiments (Figure 2). Almost the same gaseous concentrations and particle distributions at both exits of Y-tee demonstrate that the N_2O_5 source has been well mixed with the sampling flow and species concentrations at the inlet of flow tube can be accurately determined via the measurements at the other exit of Y-tee.

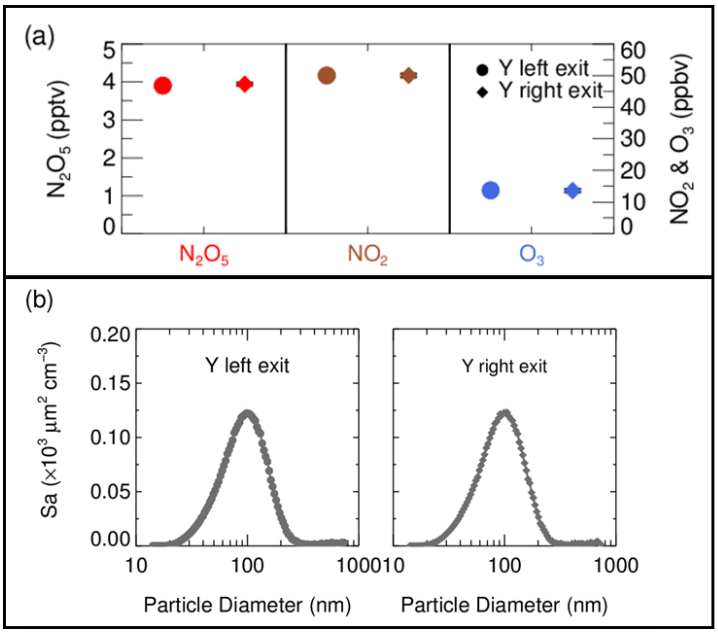

Figure 2. (a) The concentration of N_2O_5, NO_2 and O_3 in the mixture of N_2O_5 source and sampling aerosols measured at each exit of Y-tee; (b) The size distribution of Sa concentration in the mixture of N_2O_5 gas source and sampling aerosols measured at each exit of Y-tee.

2.4 Detection instruments

Instruments used in this system are listed in Table 1. A portable cavity-enhanced absorption spectrometer (CEAS) is used to measure N_2O_5 concentration (Wang et al., 2017a) at both inlet and exit of the aerosol flow tube by automatically switching the flow directions (see details in section 2.5). Briefly, the N_2O_5 is thermally decomposed to NO_3 by heating up to 130°C and then quantified according to the extinction coefficient caused by NO_3 absorption in the wavelength window from 640 to 680 nm. A Teflon polytetrafluoroethylene (PTFE) membrane

is placed in front of the CEAS to remove particles, which will be replaced with a new one every two hours by a self-designed membrane auto-changer. Laboratory tests have been conducted to quantified the transmission efficiency of N_2O_5 over the membrane (92±3%), sampling tube of CEAS (99.7%) and the inside of CEAS (93.6%). The use of a filter upstream of the CEAS and the procedures of membrane changing have been successfully applied in many field campaigns to measure ambient N_2O_5 (Brown et al., 2016;Kennedy et al., 2011;Wang et al., 2017a;Wang et al., 2017b;Wang et al., 2018a). The loss of N_2O_5 on membrane filter, sampling tube and the detection chamber inside the CEAS were corrected according to transmission efficiency. The detection limit of N_2O_5 was determined to be 2.7 pptv (1σ, 60 s) with the measurement uncertainty of 19%. A time-resolution of 60 s for N_2O_5 data acquisition is typically used to derive $\gamma(N_2O_5)$ in this study. The CEAS has been successfully applied to measure ambient N_2O_5 concentration in several field campaigns and laboratory studies (Chen et al., 2020;Wang et al., 2020a;Wang et al., 2017b;Wang et al., 2020b;Wang et al., 2018b;Wang et al., 2022).

Table 1. Performance of related instruments incorporated in the flow tube system.

Parameter	Technique	Time resolution	Detection Limit(1σ)	Accuracy
NO	Chemiluminescence[a]	1 min	200 pptv	±10%
NO_2	Chemiluminescence	1 min	300 pptv	±10%
O_3	UV photometry	1 min	500 pptv	±5%
VOCs	GC-MS/FID[b]	60 min	20-300 pptv	±15%
N_2O_5	CEAS	1 min	2.7 pptv	±19%
Sa	SMPS	5 min	-	±10%
RH&T	Sensor	1 min	-	±0.1%&±0.1K

[a] Photolytic conversion to NO through blue light before detection; [b] Gas chromatography equipped with a mass spectrometer and a flame ionization detector;

At the inlet of flow tube, NOx concentration is measured via chemiluminescence method equipped with a blue-light photolytic converter (Thermo, Model 42i) and O_3 concentration is also measured via chemiluminescence method by adding excessive NO (Teledyne API, Model T265). Both NOx and O_3 concentration are averaged to 1 min time-resolution. The size distribution of particle number density is measured at the exit of flow tube using a scanning

mobility particle sizer (SMPS, TSI 3776), which determines the total Sa concentration covering the range from 13 to 730 nm. Particles larger than this range usually contributed less than 5% of total Sa according to our previous field measurements (Chen et al., 2020) and it is included in the uncertainty analysis (see section 5). A cycle of size scanning is set to around 5 min and the derived Sa concentration is then interpolated into 1 min for further calculation. Aerosols pass through a Nafion tubing (MD-700) before entering into SMPS to reduce RH to less than 30%. The dry-state Sa is therefore corrected to wet-state at the RH inside the flow tube for particle hygroscopicity. The growth factor, $f(RH)=1+8.77\times(RH/100)^{9.74}$, used for correction is valid only when RH is within the range from 30 to 90% (Liu et al., 2013). The RH and temperature of flow are continuously measured both before entering and after leaving the flow tube by commercial sensors (Rotronic, Model HC2A-S). The averages of the values obtained at both locations are used to represent the RH and temperature inside the flow tube. In addition, ambient volatile organic compounds (VOCs) are measured in-situ alongside the aerosol flow tube system using an online gas chromatograph mass spectrometer coupled with a flame ionization detector (GCMS-FID) to derive the NO_3 reactivity to VOCs ($k_{NO3\text{-}VOCs}$) in the flow tube.

2.5 Procedures of data acquisition

The N_2O_5 concentration is acquired at both inlet and exit of the flow tube within a duty cycle via a CEAS instrument, which is different from that only at the exit of the flow tube in previous studies (Bertram et al., 2009a;Wang et al., 2018c). At each duty cycle, consisting of once HEPA inline mode for measuring k_{wall} of N_2O_5 and once HEPA bypass mode for retrieving the N_2O_5 loss on aerosols, the procedure that measuring N_2O_5 at the inlet of flow tube followed by that at the exit is executed twice with one for each mode. An exemplary case obtained during a field campaign is shown in Figure 3 to explain this procedure. Within the mode of HEPA inline, N_2O_5 data is firstly acquired at the inlet of the flow tube and then switch to the exit of the flow tube. The $k_{het}^{wo/particles}$, which is the k_{wall} of N_2O_5, can be therefore derived from a box model constrained by these N_2O_5 data (see section 3 for the model description and data processing). The same procedures are executed in the mode of HEPA bypass, except the $\gamma(N_2O_5)$ is derived

according to Eq 2. Two three-way valves controlled by a time relay were implemented to realize this procedure in order to avoid the changes of flow condition in the flow tube that could have been caused. As indicated in Figure 1, the blue arrows show the flow directions when measuring the N_2O_5 concentration at the inlet of flow tube, while the green arrows shows that for the exit of flow tube. It should be noted that the concentration of NOx and O_3 are always acquired at the inlet of the flow tube and the Sa concentration always at the exit of the flow tube during the operation.

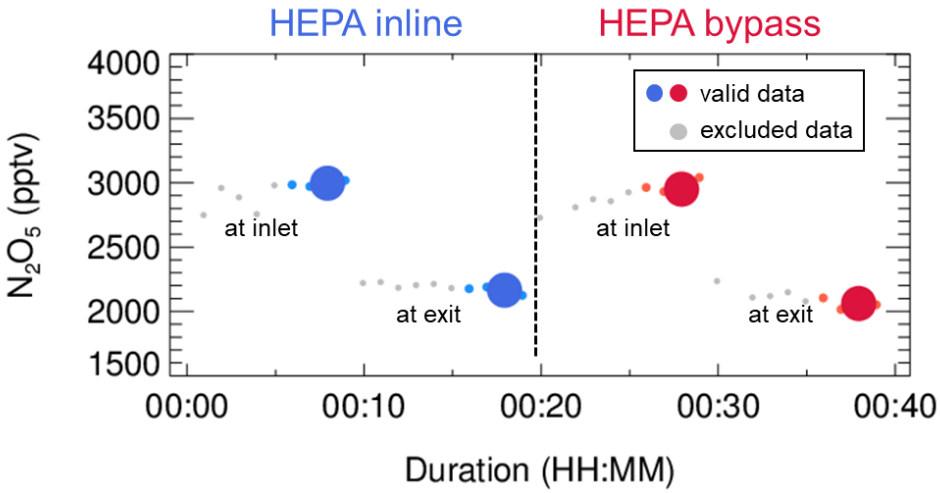

Figure 3. An exemplary case of measured N_2O_5 concentration within a duty cycle. This case was observed on the night of 13 December 2020, with average ambient Sa of 320 μm^2 cm^{-3}. The derived k_{wall} of N_2O_5 and $\gamma(N_2O_5)$ were 0.0023 s^{-1} and 0.035, respectively. The blue dots indicate N_2O_5 concentration measured under the mode of HEPA inline either at the inlet or exit of the flow tube (denoted as texts); the respective averages (blue dots of larger size) are used for deriving k_{wall} (blue square). The red dots indicate N_2O_5 concentration measured under the mode of HEPA bypass either at the inlet or exit of the flow tube; the respective averages (red dots of larger size) are used for deriving the overall rate constant of N_2O_5 loss on the wall and aerosols. The data points in gray are excluded from calculation due to unstable conditions in the flow tube.

In addition, laboratory tests were conducted to determine a suited duration for each duty cycle. During a duty cycle, the duration for each mode should last long enough to develop a stable flow condition for particles or empty particles, while a much longer duration could decrease the measurement time-resolution and leads to large uncertainty due to the fluctuations within a long time period. We measured Sa and N_2O_5 concentration continuously at the exit of

297 flow tube when sampling $(NH_4)_2SO_4$ aerosols. As shown in Figure 4, it took about 15 minutes
298 for particles to rise to a stable level from none or to decrease from a certain level to none, when
299 our system underwent mode switches. The periodical variation of N_2O_5 concentration was
300 consistent with particles. The residence time distribution (RTD) profiles (see in section 4.2)
301 also demonstrated that a pulse injection of NO_2 requires 10~15 minutes to be fully released
302 from the flow tube, which to some extent supports the 15-minute time required for complete
303 mixing of N_2O_5. As a result, a typical duration of duty cycle is composed of 40 minutes with
304 20 minutes for each mode, which is similar to that in Bertram et al. (2009). The N_2O_5
305 measurement at the exit of the flow tube in the last 5 minutes of each mode is able to represent
306 valid decays of N_2O_5 under this mode and satisfy the requirements of further data processing.

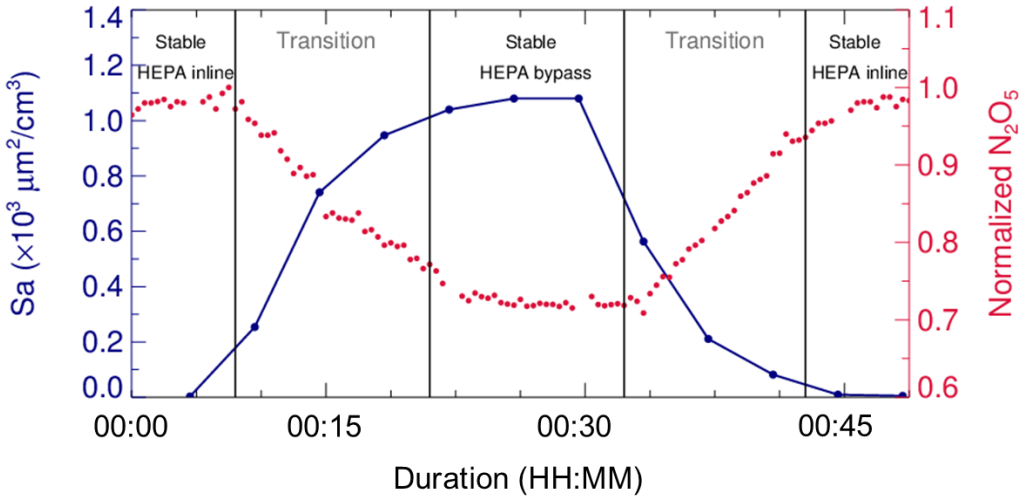

307

308 **Figure 4.** Variations of Sa and N_2O_5 concentration (normalized to peak values) measured at
309 the exit of flow tube when switching the sampling mode. The phases of species concentrations
310 in the flow tube approaching stable after a mode switch are denoted as the transition phases.

311 # 3 Box model for determination of loss rate coefficients of N_2O_5

312 ## 3.1 Method description

313 Large uncertainties were found in retrieving $\gamma(N_2O_5)$ on ambient particles according to Eq. 1
314 in a previous flow tube study (Bertram et al., 2009a), due to the dependence of homogeneous
315 reaction rates on sampling modes and the atmospheric variations of parameters related to NO_3-
316 N_2O_5 chemistry (e.g. NO, NO_2, O_3, VOCs, and RH). To minimize these influences, a time-

dependent box model constrained by the measurements of N_2O_5 concentration and other auxiliary parameters is applied to calculate loss rate coefficients of N_2O_5 under the mode of HEPA inline and bypass, respectively. The model is able to simulate the reactions related to budgets of NO_3-N_2O_5 chemistry in a dark condition, including R1, R2 and the follows:

$$NO_3 + NO \rightarrow 2\ NO_2 \qquad \text{R3}$$

$$NO_3 + \text{VOCs} \rightarrow \text{products} \qquad \text{R4}$$

$$N_2O_5 + \text{aerosols or wall} \rightarrow \text{products} \qquad \text{R5}$$

The rate constants for reactions R1 to R3 are referenced to IUPAC database. The reaction of VOCs and NO_3 is treated as pseudo-first-order with a rate constant of $k_{NO3\text{-}VOCs}$, which is the sum of rate constants for reactions of NO_3 with each VOCs scaled by the concentration of VOCs measured by GC-FID. In this work, there are 30 kinds of measured VOCs having known reaction rate constants with NO_3 included in the model (Table A1). Due to low time-resolution of VOCs measurements (1 h), the $k_{NO3\text{-}VOCs}$ is kept constant for each derivation of $\gamma(N_2O_5)$. The suppressed NO_3 concentration is expected to attenuate the influence resulted from the uncertainty of $k_{NO3\text{-}VOCs}$ (see discussion in section 5). The reaction R5 represents the loss of N_2O_5 only on the wall in the mode of HEPA inline or on the both wall and particles in the mode of HEPA bypass. The rate constant of R5 is also treated as pseudo-first-order and it is adjustable among different runs.

The same procedures of data screening and model operation are applied to both sampling and bypass modes, as shown in Figure 5. For example, in the mode of HEPA inline, the average of NO concentration less than 6 ppbv and the variation of N_2O_5 measured at the inlet of flow tube less than 10% should be validated prior to the following model operation. Under typical concentration of N_2O_5 source we used in this flow tube system, the exit concentration of N_2O_5 is detected to be under triple detection limit with initial NO large than 6 ppbv according to our laboratory tests. In ambient condition, high level of NO is usually also accompanied by rapid variation due to fresh emission, which disturbs the decay of N_2O_5 in the flow tube and leads to large uncertainty in deriving its loss rate coefficient. Excluding the cases that N_2O_5 measured at the inlet of flow tube varies exceeding 10% can further minimize the uncertainty

of N_2O_5 loss rate coefficient resulted from rapid change of NO_3 reactants (NO, VOCs). If the measured data within the duration of a sampling mode satisfies the criteria for data screening described above, the model can therefore simulate the reactions starting from the entrance of flow tube and lasting for 156 s (mean residence time) based on these data. The initial concentrations of $[NO]_{t=0}$, $[NO_2]_{t=0}$, $[O_3]_{t=0}$ and $[N_2O_5]_{t=0}$ are the averages of last-5-min values measured at the inlet of flow tube. The RH and temperature are constrained by the mean values during this sampling mode. By tuning the loss rate coefficient of N_2O_5 (k_{N2O5}) in the way of binary search, we optimized an appropriate k_{N2O5} to ensure that the N_2O_5 concentration output from the simulation is consistent with last-5-min average of N_2O_5 concentration measured at the exit of flow tube within 1 pptv. As a result, this derived k_{N2O5} (aka. $k_{het}^{wo/particles}$) is expected to be the k_{wall} of N_2O_5. The same procedures above are then applied to the data obtained in the mode of HEPA bypass, except that the derived k_{N2O5} (aka. $k_{het}^{w/particles}$) contains the loss rate coefficients of N_2O_5 on the both wall and particles. It should be noted that the above calculation for obtained data is only valid under the variation of RH less than 2% within a duty cycle and the k_{wall} of N_2O_5 can then be reasonably assumed to be constant between two successive sampling modes. Therefore, the $\gamma(N_2O_5)$ can be retrieved by the Eq 3, where the last-5-min averages of Sa concentration in the mode of HEPA bypass is used.

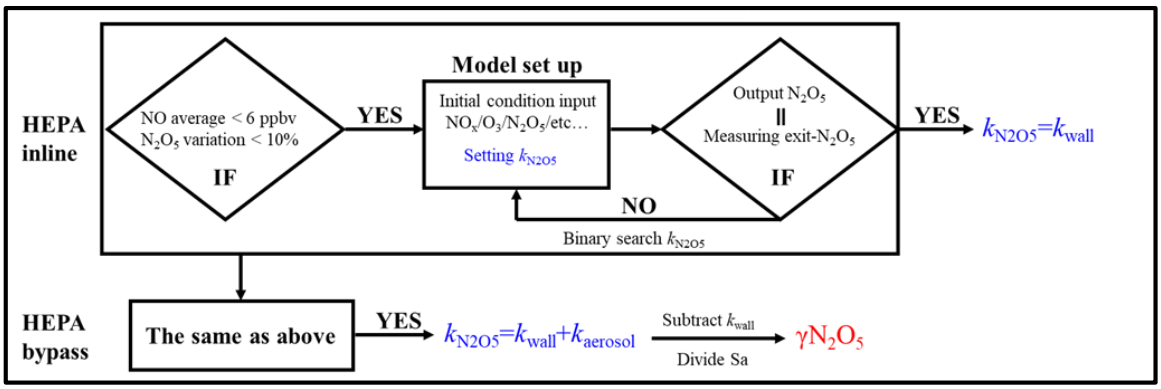

Figure 5. Flow diagram of $\gamma(N_2O_5)$ derivation through box model method.

3.2 Evaluation of the box model method

The box model method is introduced to our flow tube system to overcome the influence from homogeneous reactions and variations of air mass on $\gamma(N_2O_5)$ retrieval. A series of scenarios

were provided to evaluate the performance of box model method by both simulations and laboratory experiments. We allow NO, NO_2 and O_3 in the mixture of sampling air at the entrance of the flow tube to vary in a reasonable range, in order to develop the scenarios of different gradients of NO concentration and NO_3 production rates (PNO_3). The levels of PNO_3 was adjusted by NO_2 and O_3 concentrations and calculated from the initial NO_2 and O_3 at the entrance of the flow tube. In simulation studies, the exit concentration of N_2O_5 would be obtained from the simulated N_2O_5 evolutions with and without particles in the flow tube. To corroborate the results estimated by simulations, laboratory tests were performed on $(NH_4)_2SO_4$ aerosols to measure the exit concentration of N_2O_5 under varying NO concentration. The $\gamma(N_2O_5)$ on particles are then calculated according to Eq 1&2 or by box model method described above.

As shown in Figure 6(a), the exit concentration method ($\gamma(N_2O_5)$ exit-conc., derived directly by Eqs. 1-2) underestimates $\gamma(N_2O_5)$ and the extent of underestimation increases with PNO_3 levels in simulation tests. Similarly, the exit concentration method underestimates $\gamma(N_2O_5)$ by 50 to 60% with PNO_3 of 1.0 ppbv h^{-1} in the laboratory tests (Figure 6(b)). Noted that the $\gamma(N_2O_5)$ was determined to be at around 0.01 by box model method over the NO range from 0 to 6 ppbv, which agrees well with previous laboratory observation of $\gamma(N_2O_5)$ on $(NH_4)_2SO_4$ aerosols within uncertainty (Badger et al., 2006;Hallquist et al., 2003;Kane et al., 2001). The cause of $\gamma(N_2O_5)$ exit-conc. underestimation is mainly due to the in situ N_2O_5 production in the flow tube. With a continuous production of NO_3 via the reaction of NO_2 and O_3 and rapid heterogeneous loss of N_2O_5 in the flow tube, the equilibrium between NO_3 and N_2O_5 always shifts to the production of N_2O_5, and masking the actual amount of N_2O_5 removal. In the mode of HEPA bypass, the N_2O_5 consumes faster than the other mode due to the addition of particles, which further facilitates the N_2O_5 formation through the equilibrium. Previous studies also found similar impacts from N_2O_5 production on retrieving $\gamma(N_2O_5)$ in the aerosol flow tube (Bertram et al., 2009a;Wang et al., 2018c). However, the discrepancy of $\gamma(N_2O_5)$ derived by two methods is much less dependent on the NO concentration, at least within the prescribed range, due to relatively small ratio of NO_3/N_2O_5 in the N_2O_5 source. The absence of dependence between NO concentration and $\gamma(N_2O_5)$ also indicates that this aerosol flow

tube system can buffer against NO within the range from 0 to 6 ppbv under typical operating condition. However, this is not always the case when there is a rapid fluctuation of NO in a real atmosphere, which might lead to intractable uncertainty and is therefore excluded from further analysis according to the criteria of data screening.

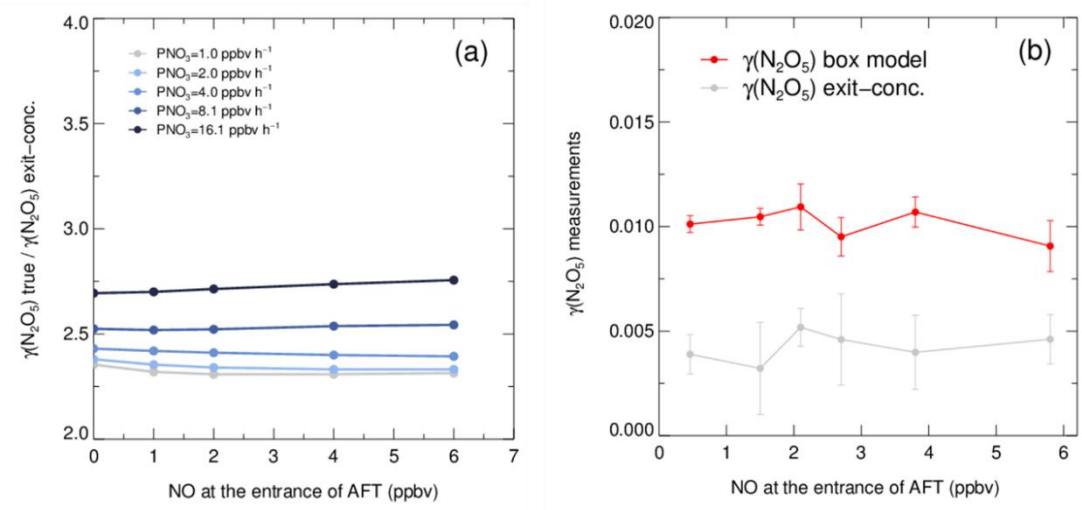

Figure 6. Simulated and laboratory tests on performance of box model method and exit concentration method for $\gamma(N_2O_5)$ derivation. (a) The ratios of given $\gamma(N_2O_5)$ ($\gamma(N_2O_5)$ true) over exit concentration derived $\gamma(N_2O_5)$ ($\gamma(N_2O_5)$ exit-conc.) determined from simulated scenarios. The $\gamma(N_2O_5)$ derived by box model method is exactly the same as $\gamma(N_2O_5)$ true. The ratios vary with NO concentration and the lines are color coded by PNO_3 values. Both NO concentration and PNO_3 represent the values at the entrance of aerosol flow tube. (b) $\gamma(N_2O_5)$ measurements on lab-generated $(NH_4)_2SO_4$ aerosols under different gradients of NO with constant RH of 50% and PNO_3 typically generated from our N_2O_5 source. The red line shows the $\gamma(N_2O_5)$ derived by box model method and gray line shows the $\gamma(N_2O_5)$ derived by exit concentration method. The NO concentrations are measured at the entrance of aerosol flow tube.

In comparison to the work by Bertram et al. (2009) and Wang et al. (2018), the combination of above box model method and the improved flow tube system in this study has progress in the following aspects. First, the dynamic quantification of k_{wall} of N_2O_5 within each duty cycle based on the constraint of sequentially measured N_2O_5 source is helpful to provide accurate data for both k_{wall} and $\gamma(N_2O_5)$ retrieval. The k_{wall} in ambient conditions could deviate from the results from laboratory tests (Figure B1) due to temperature variation and particles adsorption, which leads to large uncertainty when calculating $\gamma(N_2O_5)$ without the frequent

determination of k_{wall}. While the k_{wall} was also determined frequently in the flow tube of Wang et al. (2018), the N_2O_5 source they used for k_{wall} and $\gamma(N_2O_5)$ retrieval is an assumed stable value instead of an observed one. Second, the concentrations of initial NO, NO_2, O_3 and N_2O_5 at the entrance of the flow tube, and exit N_2O_5 are obtained through programed cyclic measurements in this work, which can reduce the uncertainties by adding the model constraints. It is different from the iterative box model used in Wang et al. (2018) as we enable a straightforward simulation of NO_3-N_2O_5 chemistry occurring in the flow tube, instead of estimating the initial NO_2 and O_3 with assumed NO profile and stable N_2O_5 source based on backward simulations. In ambient conditions, the initial N_2O_5 concentration can be largely influenced by air mass conditions (especially NO concentration and temperature). Figure B2(a) presents box whisker plot of N_2O_5 and NO concentration at the flow tube entrance during a field campaign, which shows a much larger variation of N_2O_5 than in lab condition (<1%). As a result, the box model would underestimate $\gamma(N_2O_5)$ by using a fixed initial N_2O_5 concentration under certain circumstances (Figure B2(b)). Third, we simulate NO_3-N_2O_5 relationship via specific reactions rather than approximating it in equilibrium and introducing the equilibrium coefficient (*K*eq) into calculation. Calculating NO_3 or N_2O_5 concentration by *K*eq could induce large bias (up to 90%) under the high aerosol loading and low temperature (Chen et al., 2021).

4 Laboratory characterizations

4.1 Particle transmission efficiency

The transmission efficiency of particles in the sampling module and flow tube are estimated respectively in Figure 7. In the laboratory, pure ammonia nitrate ($(NH_4)_2SO_4$) aerosols were generated from an atomizer loading with 0.1 M $(NH_4)_2SO_4$ solution. The RH and concentration of produced aerosols flow was conditioned in a glass bottle (~2 L) by introducing a humidified dilution flow of ultrahigh-purity N_2. As a result, aerosols in different concentrations (1000~4500 μm^2 cm^{-3}) and under a range of RH (20~70%) were applied to test the transmission efficiency. Figure 7(a) shows the loss of total Sa concentration in the sampling

module and flow tube are 8±1% and 10±2% on average, respectively. We found that the fraction of particles loss is mainly caused by particles smaller than 100 nm. This is most likely due to the turbulence generated by static mixer and the recirculation in the flow tube. Large particles are prone to stay within the main flow direction, whereas small particles readily adsorb on the walls by the entrainment of turbulence or recirculation. In addition, the particles distribution measured at the exit of flow tube with HEPA inline (gray line in Figure 7(a)) demonstrated its capability of removing almost all particles (>99.5%) at the typical flow rate. The same transmission efficiency was also found on ambient aerosols (Figure 7(b)) as that on laboratory-generated aerosols. The results we obtained from above particle transmission experiments are similar to the findings of Bertram et al. (2009).

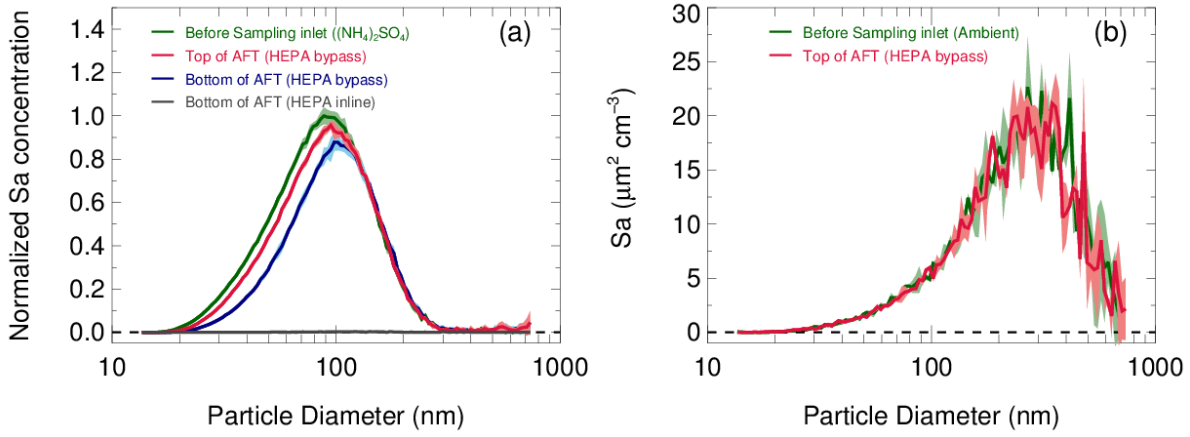

Figure 7. (a) Particles transmission determined by sampling laboratory-generated $(NH_4)_2SO_4$ aerosols. Aerosols at different concentrations and RH levels are used in experiments and the size distribution of Sa concentration are normalized to the peak values. The normalized size distribution of Sa concentration measured before sampling inlet (green line), at the inlet of flow tube with HEPA bypass (red line) and at the bottom of flow tube with HEPA bypass (blue line) are shown respectively. Under the mode of HEPA inline, the Sa concentration was almost zero at the bottom of flow tube (gray line). The shadows indicate the standard deviations of the normalized Sa concentration for all experiments. (b) Particles transmission determined by sampling ambient particles.

4.2 Residence time in the flow tube

The method of residence time distribution (RTD) was applied to estimate the average reaction time of the gas species in the flow tube (residence time). In comparison to ideal plug flow, the

RTD method can better describe actual behavior of the flow in practice and determine the mean residence time more accurately (Danckwerts, 1953). Several studies have also used this RTD method to determine the residence time in the flow tube (Huang et al., 2017;Wang et al., 2018c;Lambe et al., 2011).

The RTD profiles were obtained by introducing a 2 s pulse of NO_2 gas diluted in N_2 into the flow tube under RH less than 1%. NO_2 is relatively inert against the flow tube wall coated with FEP and was measured at the exit of the flow tube by a CEAS (Li et al., 2021) at high time-resolution (2 Hz). A three-way solenoid valve combined with a time relay was implemented to control the pulse in order to avoid the disturbance on flow condition from the injection. Experiments were performed under typical operation. The mean residence time (t_{ave}) can be derived from the each RTD profile according to Eq. 4,

$$t_{ave} = \frac{\sum_{i=0} C_i \times t_i}{\sum_{i=0} C_i}, \quad \text{Eq. 4}$$

where the C_i is the concentration of NO_2 recorded at the time step t_i. From the RTD profiles of NO_2 injection experiments in Figure 8, the determined t_{ave} was 156±3 s. This value is 19% less than the space time (τ_{space}, flow tube volume divided by operation flow rate, 192.6 s). It has also been found that the assumption of ideal plug flow overestimated the residence time in previous flow tube experiments (Lambe et al., 2011;Huang et al., 2017;Wang et al., 2018c), which could lead to underestimation of the derived k_{N2O5}. The residence time of current set up is designed for investigating $\gamma(N_2O_5)$ in typical episode days with medium to high aerosol loadings (the Sa concentration usually larger than 500 $um^2\ cm^{-3}$) in polluted regions. As shown in Section 5, the detection limit of this system is 6.4×10^{-4} with Sa of 500 $um^2\ cm^{-3}$, which is well below the most of previous ambient $\gamma(N_2O_5)$ results ranging from 1×10^{-3} to >0.1 in polluted regions of China (Wang et al., 2020a;Wang et al., 2017d;Wang et al., 2017e;Xia et al., 2019). The residence time determined in this work is also slightly higher than 149 s that reported in a previous work focusing on investigating $\gamma(N_2O_5)$ in polluted regions(Wang et al., 2018c). In addition, the residence time for this flow tube can be extended to over 300 s to satisfy the $\gamma(N_2O_5)$ measurement requirements under low Sa by reducing the flow rate of air passing through, which is controlled by an extra pump.

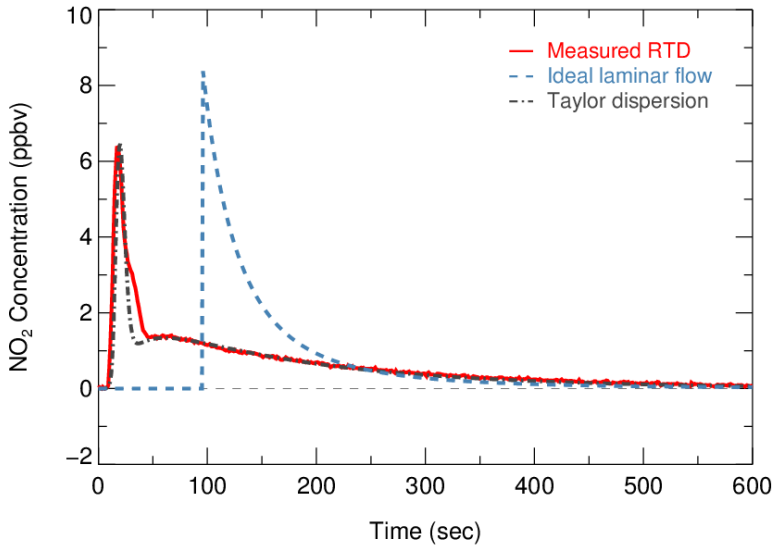

Figure 8. Residence time distribution derived by sampling NO_2 gas. Red solid line indicates the measured RTD profiles. The calculated RTD of ideal laminar flow (without dispersions) and the Taylor dispersion model fitted to measurements are shown as blue dash line and dot-dash line, respectively.

Two theoretical RTDs were calculated, namely ideal laminar flow and Taylor diffusion, besides the measured RTD, intending to reflect the fluid field inside the flow tube. The ideal laminar flow describes the flow without dispersion. The velocity profile of ideal laminar flow is parabolic, with the fluid in the center of the tube moving the fastest. According to the following Eq. 5, the RTD of ideal laminar flow is scaled by the integrated concentration of NO_2 and presented as the blue dash line in Figure 8.

$$\begin{cases} 0, & t < 0.5\tau_{space} \\ \dfrac{{\tau_{space}}^2}{2t^3}, & t \geq 0.5\tau_{space} \end{cases}, \qquad \text{Eq. 5}$$

While the determined *Re* is well within the laminar flow threshold, the measured RTD occurs earlier than theoretical laminar flow condition and exhibits a broaden distribution. The discrepancy between them indicates that the dispersions or potential secondary flows could dominate the flow regime. Instead, an improved Taylor dispersion model (shown as the gray dot-dash line in Figure 8) is able to reproduce the measured RTD, which was previously implemented in the characterization of photooxidation flow reactors (Lambe et al., 2011). Two flow patterns with distinct effective diffusivities (0.02 and 0.51 derived from best fit) were considered in this dispersion model. An implication from the characteristics of the model is

that two flow components consist of the flow regime: a direct flow path through the flow tube with less diffusion and a secondary flow path representing the recirculation in the dead zone that induced by temperature gradient and significant diffusions (Huang et al., 2017).

4.3 N_2O_5 wall loss

The stainless-steel flow tube in this study is electro-polished and coated by FEP inside to reduce the loss of N_2O_5 and particles on the wall in the meantime. An electro-polished surface could enhance the homogeneity of FEP-coating and reduce the adsorption of H_2O molecule to the wall, which influences the loss of N_2O_5. It has been found that the k_{wall} of N_2O_5 increases with the RH (Bertram et al., 2009a;Wang et al., 2018c). Therefore, a less change in k_{wall} of N_2O_5 from RH helps to minimize the uncertainty induced by fluctuations of RH within a duty cycle. Laboratory tests were conducted to quantify the k_{wall} of N_2O_5 under different levels of RH with HEPA inline. As shown in Figure 9, the k_{wall} of N_2O_5 gradually increase from 0.002 s^{-1} in a dry condition to 0.006 s^{-1} when RH is 70%. The level of k_{wall} is less than the result of Wang et al. (2018c) but higher than Bertram et al. (2009a) as indicated in Table 2. In addition, the flow tube was rinsed with deionized water every week during the field campaigns to remove the build-up of particles, which might increase the hygroscopicity of the internal surface and thus the k_{wall} of N_2O_5 in a wet condition. Uncertainty in $\gamma(N_2O_5)$ derivation resulted from the variation of k_{wall} related to RH is discussed in section 5.

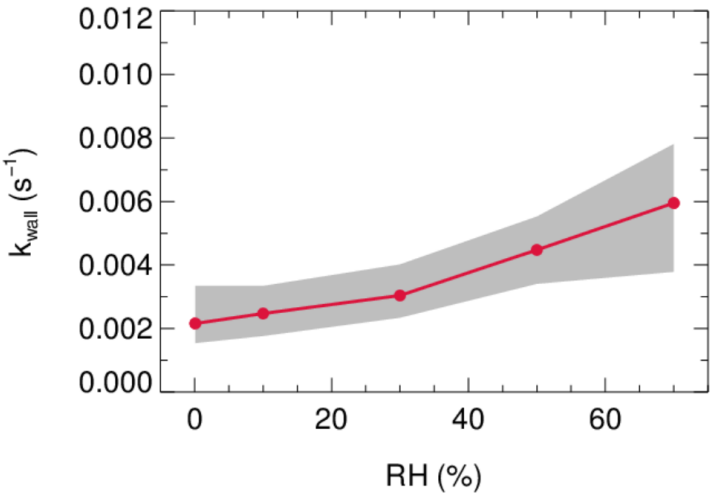

Figure 9. The dependence of pseudo-first-order wall loss coefficient (k_{wall}) of N_2O_5 in the FEP-coated aerosol flow tube.

Table 2. Summary of the k_{wall} of N_2O_5 for the existing aerosol flow tube deployed in field campaigns.

RH range	k_{wall} range ($\times 10^{-3}$ s^{-1})	References
5~50%	0.5~3	Bertram et al., 2009
20~70%	4~9	Wang et al., 2018
0~70%	2~6	This work

4.4 Demonstration of $\gamma(N_2O_5)$ measurements on model particles

$\gamma(N_2O_5)$ measurements by current aerosol flow tube system equipped with box model method were performed on lab-generated $(NH_4)_2SO_4$ aerosols over a range of RH. The system was operated at room temperature of 295K with N_2O_5 concentration of 4.0 ppbv at the entrance of flow tube. We conditioned the RH of generated aerosols by introducing dry N_2 gas dilution, which could decrease the RH level down to 10~55%, starting from over 95% where $(NH_4)_2SO_4$ aerosols are expected to be in aqueous state. The resulting Sa concentrations of aerosols were around 600 $\mu m^2 \cdot cm^{-3}$. As shown in Figure 10, the observed $\gamma(N_2O_5)$ values were below 0.01 when RH was within 40% and significantly rose up to 0.02 with higher RH. The dependence of $\gamma(N_2O_5)$ on RH and the exact values are well consistent with previous laboratory results on $(NH_4)_2SO_4$ aerosols (Badger et al., 2006;Hallquist et al., 2003;Hu and Abbatt, 1997;Kane et al., 2001;Mozurkewich and Calvert, 1988), which shows that the setup of our instrument has good practicability. A large standard deviation of $\gamma(N_2O_5)$ found at RH of 39% is possibly due to the unstable phase transition of $(NH_4)_2SO_4$ particles, as its efflorescence RH is reportedly from 35 to 48% (Martin, 2000).

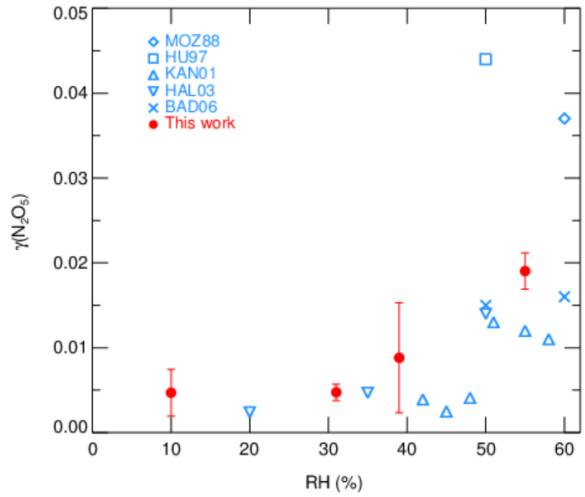

Figure 10. The dependence of $\gamma(N_2O_5)$ on RH for laboratory-generated $(NH_4)_2SO_4$ aerosols. The red points with standard deviations represent the values measured by current aerosol flow tube system in this work. Previously reported values are indicated in blue marks.

5 Uncertainty analysis and detection limit

The uncertainty of $\gamma(N_2O_5)$ is in relevance to the measurement uncertainties of each instrument and rapid fluctuations of various parameters. As outlined before, the 5-min averages of N_2O_5 concentration measured at the inlet and exit of the flow tube were used for calculating $\gamma(N_2O_5)$ via the box model method. The potential variations within these selected time periods would therefore lead to relative errors. For example, the variations of N_2O_5 concentration is resulted majorly from the rapid changes of ambient NO and less from variations of VOCs, NO_2, O_3 as well as N_2O_5 gas source itself (1% in 24 hours). A cutoff of 10% for N_2O_5 variation was implemented to filter out the air mass that was too unstable for valid analysis, according to our prescribed criteria of data screening. It consequently leads to 10% uncertainty in the average of N_2O_5 and can translate into a deviation of 2% in $\gamma(N_2O_5)$ with the $\gamma(N_2O_5)$ at 0.02, Sa at 800 $\mu m^2 \cdot cm^{-3}$ and other parameters (shown in Table 3) representing the typical inlet values measured during the field campaign (described in section 6). Similarly, cases that over 2% variation in RH exists between the HEPA inline and bypass mode are excluded from analysis, owing to its significant influence on k_{wall} of N_2O_5 in the flow tube. By assuming a consistent k_{wall} in successive sampling modes, the potential variations in RH could lead to uncertainty in

570 $\gamma(N_2O_5)$ from $\pm8\times10^{-4}$ at RH of 20% to $\pm2\times10^{-3}$ at RH of 70%, respectively, with the Sa at
571 800 μm^2 cm^{-3}. In addition, the $k_{NO3\text{-}VOCs}$ is treated as constant in a duty cycle due to the limit
572 of time resolution of VOCs measurements. A variation of ±0.01 s^{-1} in $k_{NO3\text{-}VOCs}$ only induces
573 less than ±1% uncertainty in $\gamma(N_2O_5)$ for more than 95% cases obtained during the field
574 campaign. All the impacts from inherent instruments uncertainties and variations of different
575 parameters are thereby considered in Monte Carlo simulations to assess the overall uncertainty
576 of $\gamma(N_2O_5)$. The basic simulation is initialized with the typical conditions measured at the inlet
577 of the flow tube during the field campaign and repeatedly performs the procedures of
578 determining $\gamma(N_2O_5)$ via the box model method 1000 times. In each run, all parameters were
579 allowed to vary independently within a prescribed range. The basic simulation condition and
580 variation range are presented in Table 3.

581 **Table 3.** Parameters involved in the Monte Carlo simulations.

Parameters	Value [a]	Variation range [b]
NO	1 ppbv	±10%
NO_2	70 ppbv	±10%
O_3	10 ppbv	±5%
Inlet N_2O_5	4 ppbv	±19%
Exit N_2O_5 [c]	2.2 ppbv	±19%
Temperature	273 K	±0.1 K
RH [d]	30 %	±1%
$k_{NO3\text{-}VOCs}$	0.01 s^{-1}	±0.01 s^{-1}

582 [a] Values used for initializing Monte Carlo simulations in a basic scenario; [b] Ranges within
583 which each parameter can vary independently; [c] Determined from the case that $\gamma(N_2O_5)$ is at
584 0.02, Sa is at 800 $\mu m^2 \cdot cm^{-3}$ and other parameters are shown in this table; [d] The RH and its
585 variation can be transformed into values in k_{wall} of N_2O_5 via the fitting function derived from
586 Figure 9.

587 The resulting $\gamma(N_2O_5)$ values from Monte Carlo simulations under the basic scenario are
588 shown as frequency distributions in Figure 11(a). This distribution can be fitted by a Gaussian
589 function and the standard deviation (1σ) of Gaussian distribution is regarded as the overall

uncertainty of $\gamma(N_2O_5)$, which is $\pm 9 \times 10^{-4}$ (4.5% relative to true $\gamma(N_2O_5)$). The uncertainty of Sa measurements and unmeasured particles larger than 730 nm (usually less than 5% of total Sa) would together introduce an extra 16% uncertainty to $\gamma(N_2O_5)$.

We further found that the uncertainty of $\gamma(N_2O_5)$ could be sensitive to the measurement conditions. With higher O_3, potential variations of NO and $k_{NO3\text{-}VOCs}$ will induce larger uncertainty of $\gamma(N_2O_5)$ (Figure 11(b)), as it enhances the abundance of NO_3 and N_2O_5. In comparison, the low O_3 in the basic scenario suppressed the side formation of NO_3 in the flow tube, limiting the aggravation of $\gamma(N_2O_5)$ uncertainty from the increase of NO and NO_2. The $\gamma(N_2O_5)$ uncertainty is also positive correlated with RH and T. As is discussed before, the k_{wall} of N_2O_5 increases with RH level, which can amplify the potential bias of k_{wall} at a higher RH level. The equilibrium between NO_3 and N_2O_5 shifts towards the decomposition of N_2O_5 at higher T, leading to larger uncertainty of $\gamma(N_2O_5)$ caused by potential variations of NO and $k_{NO3\text{-}VOCs}$. The overall uncertainty of $\gamma(N_2O_5)$ therefore rises to 8.2% at the RH of 70% and to 14.4% at the temperature of 293K (Figure 11(c)), with NO, NO_2, O_3, $\gamma(N_2O_5)$ and Sa keeping the same as the basic scenario. In addition, Monte Carlo simulations were also performed for different $\gamma(N_2O_5)$ values ranging from 0.01 to 0.08. The uncertainty of $\gamma(N_2O_5)$ clearly decreased with the $\gamma(N_2O_5)$ (Figure 11(d)). A lower $\gamma(N_2O_5)$ weaken the impacts N_2O_5 uptakes has on the budgets of NO_3 and N_2O_5, which causes the $\gamma(N_2O_5)$ derivation to be more susceptible to uncertainties of other parameters and then increases the uncertainty of $\gamma(N_2O_5)$.

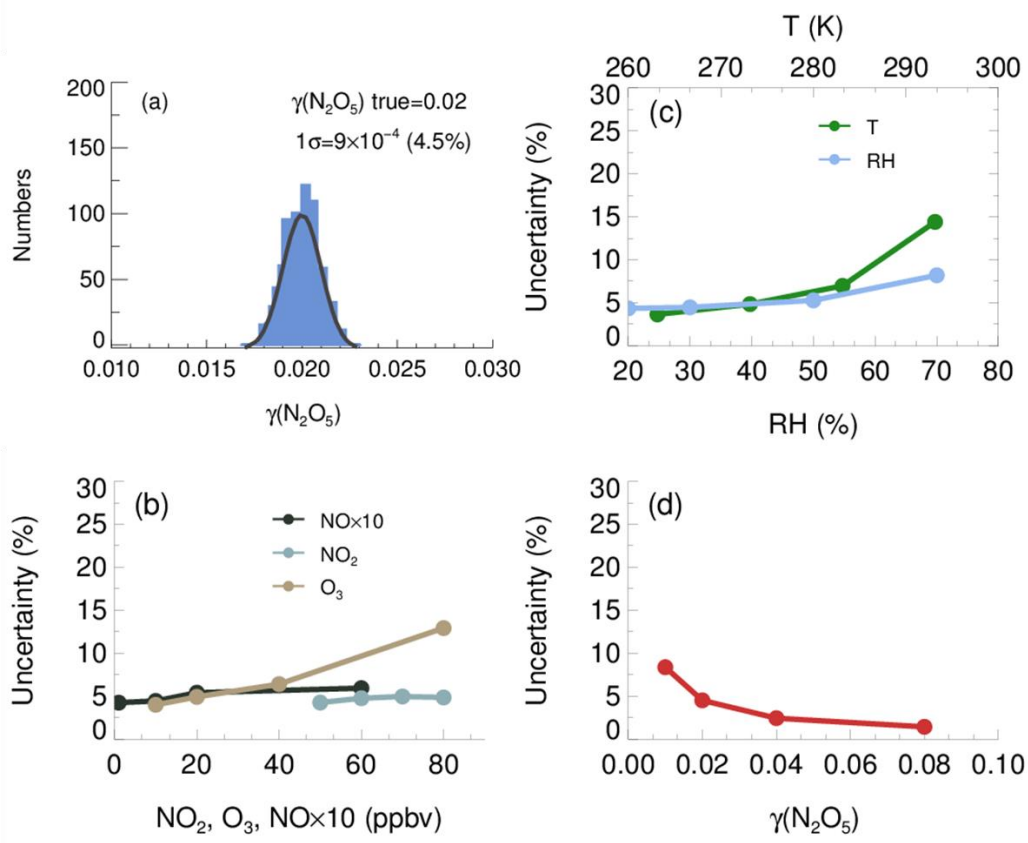

Figure 11. The uncertainty of $\gamma(N_2O_5)$ determined from the Monte Carlo simulations. (a) Histogram distribution of $\gamma(N_2O_5)$ generated from a Monte Carlo simulation (1000 single runs) in the basic scenario (shown as Table 3), where the overall uncertainty of $\gamma(N_2O_5)$ was determined to be $\pm 9 \times 10^{-4}$; (b) dependence of the uncertainty of $\gamma(N_2O_5)$ on NO, NO_2 as well as O_3; (c) dependence of the uncertainty of $\gamma(N_2O_5)$ on RH and T; (d) dependence of the $\gamma(N_2O_5)$ uncertainty on $\gamma(N_2O_5)$ level.

In addition, the mean residence time used in the box model method could bias the retrieved $\gamma(N_2O_5)$ due to the non-normal distribution of residence time with a discernable tail. The reactants entrained by those slower streamlines close to the wall will take much longer time to reach the exit of the flow tube than that by the centerline. In order to evaluate the uncertainty caused by the distribution of residence time, we first performed simulations of N_2O_5 decay in the flow tube under the basic scenarios and calculate the exit N_2O_5 concentration according to the probability distribution function derived from RTD profile. Then the $\gamma(N_2O_5)$ can be retrieved from the box model method running for the duration of mean residence time, constrained by this calculated exit N_2O_5 concentration. The result shows that the use of mean residence time produces 32% underestimation of $\gamma(N_2O_5)$ in the basic scenario. The extent of

underestimation is most sensitive to the level of $\gamma(N_2O_5)$ and RH. In short, when taking all the factors and their corresponding varying ranges discussed above into consideration, the overall uncertainty of $\gamma(N_2O_5)$ determined from Monte Carlo simulations is in the range of 16-43%.

In order to determine the detection limit of the current aerosol tube system, the continuous blank measurements in zero air were performed with settled operation procedures. Within per duty cycle (40 minutes), one k_{wall} of N_2O_5 and one $\gamma(N_2O_5)$ can be derived in pair. In total, we obtained 56 sets of result. The detection limit of k_{N2O5} on aerosols is 2.1×10^{-5} s^{-1}, derived from 1σ of the Gaussian function fitted to this distribution. It is equivalent to 0.0016 for the detection limit of $\gamma(N_2O_5)$ with a low Sa condition of 200 μm^2 cm^{-3} (Figure 12(a)), and 0.00064 for the detection limit of $\gamma(N_2O_5)$ with a moderate Sa condition of 500 μm^2 cm^{-3} (Figure 12(b)). This result indicates that the flow tube system has capability of quantifying $\gamma(N_2O_5)$ for most cases even under a low aerosol-loading environment.

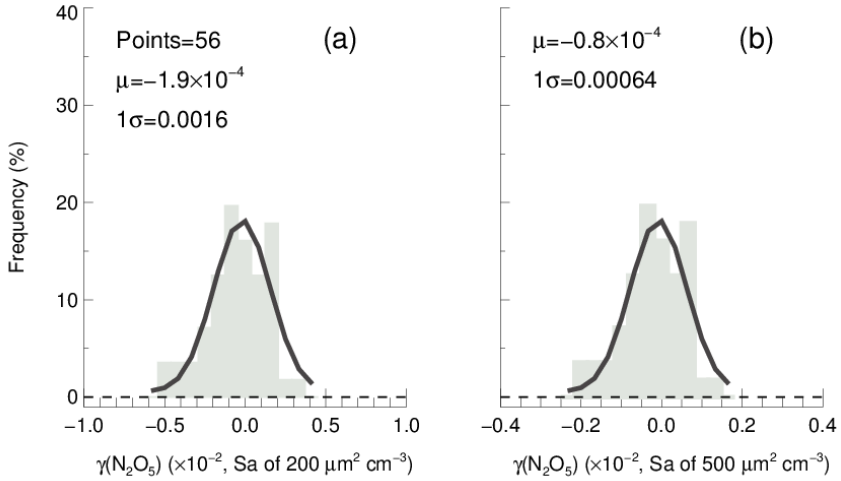

Figure 12. The $\gamma(N_2O_5)$ derived from blank measurements in histogram distribution plot. The $\gamma(N_2O_5)$ was calculated from k_{N2O5} by Eq 2 with Sa of (a) 200 μm^2 cm^{-3} and (b) 500 μm^2 cm^{-3}, respectively, under the temperature of 293K. The Gaussian function is fitted to the distribution and plotted in black line. The 1σ from Gaussian fit is regarded as the detection limit.

6 Performance in the field campaign

The aerosol flow tube system was successfully deployed to measure $\gamma(N_2O_5)$ on ambient aerosols in Beijing lasting for 20 days during the December of 2020. The sampling site was at

646 the campus of Peking University, which is located in the city center of Beijing surrounded by
647 major roads with heavy traffic. Therefore, this site represents an area with large amount of
648 fresh emission of NOx and other anthropogenic sources. The system was mounted in the top
649 floor of a building, about 15 m height above the ground. The sampling manifold was placed
650 in open air and the ambient aerosols could directly enter the inlet of the manifold without
651 additional sampling tubes. During the period of measurement, the averages of ambient
652 temperature, RH, NO, NO_2, O_3 and Sa were 273 ± 3 K, 25 ± 12 %, 23 ± 36 ppbv, 23 ± 12 ppbv,
653 16 ± 15 ppbv and 409 ± 249 μm^2 cm^{-3}, respectively. The NO and Sa levels could vary by 2
654 orders of magnitude due to the periodical switch between clean air mass from the north and
655 pollutants accumulated by local emission.

656 A total of 99 valid $\gamma(N_2O_5)$ values were determined from the measurements based on the
657 criteria of data screening described in section 3.1. We found that $\gamma(N_2O_5)$ was 0.042±0.026 on
658 average with a median of 0.035, ranging from 0.0045 to 0.12 (Figure 13). These results are
659 comparable to that previously determined in the North of China using various different
660 methods (Wang et al., 2017b;Wang et al., 2018b;Wang et al., 2017d;Wang et al., 2017e;Xia et
661 al., 2019;Yu et al., 2020a). The k_{wall} of N_2O_5 corresponding to valid $\gamma(N_2O_5)$ measurements
662 was rather stable at an average of 0.0021±0.0007 s^{-1}, which was consistent with the values
663 determined at similar RH levels in the laboratory tests. It somehow reflected the robustness of
664 the status of the flow tube system and the derived results.

665 In the current system, the N_2O_5 concentrations measured at both entrance and exit of the
666 flow tube are sensitive to the NO fluctuations within the timescale of one sampling mode,
667 which can induce large uncertainty on calculating $\gamma(N_2O_5)$. With our stringent criteria of data
668 screening, the cases of drastic NO fluctuations were excluded from the analysis. Hence, the
669 majority of valid $\gamma(N_2O_5)$ for this campaign were obtained during the periods of the NO below
670 2 ppbv, when the clean air mass was dominant at this urban site. Meanwhile, the Sa
671 concentration within clean episodes were also lower than other periods, with an average of
672 159 μm^2 cm^{-3}. The derived k_{N2O5} ranged from 2.1×10^{-5} to 1.6×10^{-3} s^{-1} well above the
673 detection limit, which demonstrated the robustness of results even subject to low ambient Sa
674 conditions. In order to improve the applicability of $\gamma(N_2O_5)$ measurements, future

development is suggested to prioritize the reduction or removal of NO level (at least the fluctuation of NO) in the sampling system before the entrance of flow tube without the cost of particles transmission efficiency.

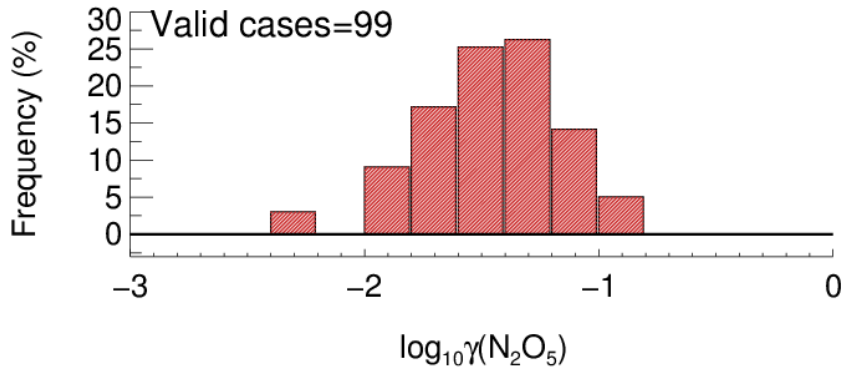

Figure 13. The histogram distribution of measured $\gamma(N_2O_5)$ for valid cases.

7 Summary and conclusion

We report a new development of an aerosol flow tube system coupled with detailed box model to derive $\gamma(N_2O_5)$ directly on ambient aerosols. The unique feature of this system is that the sequential N_2O_5 measurement at the both ends of flow tube was applied to improve the accuracy in quantifying $\gamma(N_2O_5)$, by taking it as a constraint for the box model to reproduce the decay of introduced N_2O_5 gas source in the flow tube. With the consideration of detailed chemistry related to N_2O_5, the proposed approach was testified to refrain from the interference of side reactions, induced by the additional N_2O_5 generation, NO titration in the flow tube and variations of air masses between successive sampling modes.

A series of laboratory tests were performed to characterize factors affecting $\gamma(N_2O_5)$ derivation and demonstrate its applicability on $(NH_4)_2SO_4$ aerosols. The uncertainties associated with instruments used in the system and potential fluctuations of various parameters were thoroughly discussed in the uncertainty analysis, and we estimated the overall uncertainty of $\gamma(N_2O_5)$ to be 16-43% which is subject to NO, NO_2, O_3, meteorological parameters, residence time and $\gamma(N_2O_5)$ value itself. The detection limit of $\gamma(N_2O_5)$ was quantified to be 0.0016 at the aerosol surface concentration (Sa) of 200 μm^2 cm^{-3}. We deployed this system for field observations of $\gamma(N_2O_5)$ at an urban site in Beijing, where strong anthropogenic emission

and frequent switch of air mass were encountered. The obtained $\gamma(N_2O_5)$ was in comparable level to previously reported values in northern China and demonstrated the robustness of this system during low NO episodes. Further investigations on N_2O_5 heterogeneous chemistry for both laboratory-generated and ambient particles are also available by the introduced approach.

Appendix A: Measured VOCs used to calculate NO_3 reactivity in the box model method

A total of 59 kinds of VOCs were measured by GC-FID-MS in this work, half of which had known rate constants that can be used to parameterize the reaction of NO_3 with VOCs (mainly compose of alkenes and aromatics) in $\gamma(N_2O_5)$ retrieval by box model method (see also section 3). Their rate constants were obtained from MCM331 or IUPAC and the values at 298K are listed in Table A1.

Table A1. VOCs used to calculate NO_3 reactivity (k_{NO3}) in the box model method

Species	k_{NO3}(298 K)	Species	k_{NO3}(298 K)
METHANE	1D-18 [b]	TRANS-2-PENTENE	3.70D-13 [a]
ETHANE	1D-17 [b]	1-HEXENE	1.20D-14 [a]
PROPANE	7D-17 [b]	1-3 BUTADIENE	1.03D-13 [a]
N-BUTANE	4.6D-17 [b]	ISOPRENE	7.0D-13 [b]
I-BUTANE	1.1D-16 [b]	STYRENE	1.50D-12 [a]
ETHYLENE	2.1D-16[b]	ETHYNE	1D-16 [b]
PROPYLENE	9.5D-15[b]	BENZENE	3D-17 [b]
1-BUTENE	1.3D-14[b]	TOLUENE	7.8D-17 [b]
CIS-2-BUTENE	3.50D-13 [a]	O-XYLENE	4.10D-16 [a]
TRANS-2-BUTENE	3.90D-13 [a]	M-XYLENE	2.60D-16 [a]
I-BUTENE	3.4D-13 [b]	P-XYLENE	5.00D-16 [a]
1-PENTENE	1.20D-14 [a]	ETHYL BENZENE	1.20D-16 [a]
CIS-2-PENTENE	3.70D-13 [a]	N-PROPYL BENZENE	1.40D-16 [a]

Note: a. MCM; b. IUPAC

Appendix B: Evaluations of box model method by ambient data.

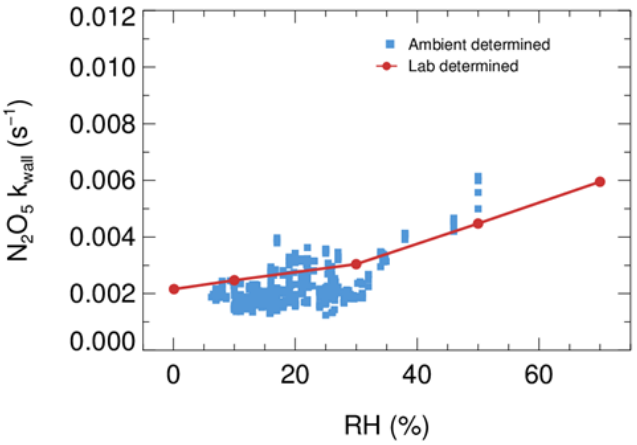

Figure B1. The derived dependence of N_2O_5 wall loss on RH at laboratory condition (red dots) and field measurement (blue square)

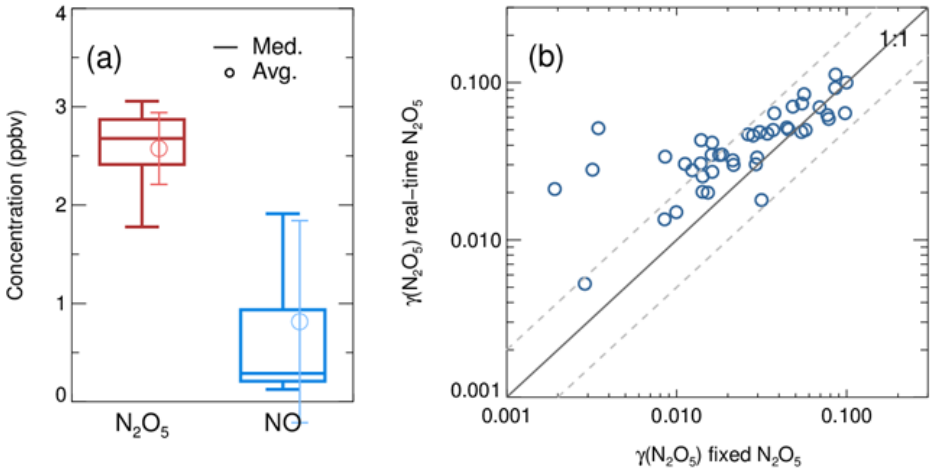

Figure B2. (a) the box whisker of N_2O_5 source and NO measured before the entrance; (b) the inter-comparison of derived N_2O_5 uptake coefficient by using a fixed initial N_2O_5 and a dynamic measured N_2O_5 at the flow tube entrance in the iterative box model.

Code/Data availability. The datasets used in this study are available from the corresponding author upon request (wanghch27@mail.sysu.edu.cn; k.lu@pku.edu.cn).

Author contributions. K.D.L. and H.C.W. designed the study. X.R.C and H.C.W. analyzed the data and wrote the paper with input from K.D.L.

Competing interests. The authors declare that they have no conflicts of interest.

Acknowledgments. This project is supported by the National Natural Science Foundation of China (21976006, 42175111); the Beijing Municipal Natural Science Foundation for Distinguished Young Scholars (JQ19031); National State Environmental Protection Key Laboratory of Formation and Prevention of Urban Air Pollution Complex (CX2020080578); the special fund of the State Key Joint Laboratory of Environment Simulation and Pollution Control (21K02ESPCP); the National Research Program for Key Issue in Air Pollution Control (DQGG0103-01, 2019YFC0214800). Thanks for the data contributed by field campaign team.

References

Ahern, A. T., Goldberger, L., Jahl, L., Thornton, J., and Sullivan, R. C.: Production of N2O5 and ClNO2 through Nocturnal Processing of Biomass-Burning Aerosol, Environmental Science & Technology, 52, 550-559, 10.1021/acs.est.7b04386, 2018.

Anttila, T., Kiendler-Scharr, A., Tillmann, R., and Mentel, T. F.: On the reactive uptake of gaseous compounds by organic-coated aqueous aerosols: Theoretical analysis and application to the heterogeneous hydrolysis of N2O5, J. Phys. Chem. A, 110, 10435-10443, 10.1021/jp062403c, 2006.

Baasandorj, M., Hoch, S. W., Bares, R., Lin, J. C., Brown, S. S., Millet, D. B., Martin, R., Kelly, K., Zarzana, K. J., Whiteman, C. D., Dube, W. P., Tonnesen, G., Jaramillo, I. C., and Sohl, J.: Coupling between Chemical and Meteorological Processes under Persistent Cold-Air Pool Conditions: Evolution of Wintertime PM2.5 Pollution Events and N2O5 Observations in Utah's Salt Lake Valley, Environmental Science & Technology, 51, 5941-5950, 10.1021/acs.est.6b06603, 2017.

Badger, C. L., Griffiths, P. T., George, I., Abbatt, J. P. D., and Cox, R. A.: Reactive uptake of N2O5 by aerosol particles containing mixtures of humic acid and ammonium sulfate, J. Phys. Chem. A, 110, 6986-6994, 10.1021/jp0562678, 2006.

Bertram, A. K., Martin, S. T., Hanna, S. J., Smith, M. L., Bodsworth, A., Chen, Q., Kuwata, M., Liu, A., You, Y., and Zorn, S. R.: Predicting the relative humidities of liquid-liquid phase separation, efflorescence, and deliquescence of mixed particles of ammonium sulfate, organic material, and water using the organic-to-sulfate mass ratio of the particle and the oxygen-to-carbon elemental ratio of the organic component, Atmos. Chem. Phys., 11, 10995-11006, 10.5194/acp-11-10995-2011, 2011.

Bertram, T., and Thornton, J.: Toward a general parameterization of N 2 O 5 reactivity on aqueous particles: the competing effects of particle liquid water, nitrate and chloride, Atmos. Chem. Phys., 9, 8351-8363, 2009a.

Bertram, T. H., and Thornton, J. A.: Toward a general parameterization of N2O5 reactivity on aqueous particles: the competing effects of particle liquid water, nitrate and chloride, Atmos. Chem. Phys., 9, 8351-8363, 10.5194/acp-9-8351-2009, 2009b.

Bertram, T. H., Thornton, J. A., and Riedel, T. P.: An experimental technique for the direct measurement of N2O5 reactivity on ambient particles, Atmospheric Measurement Techniques, 2, 231-242, 10.5194/amt-2-231-2009, 2009a.

Bertram, T. H., Thornton, J. A., Riedel, T. P., Middlebrook, A. M., Bahreini, R., Bates, T. S., Quinn, P. K., and Coffman, D. J.: Direct observations of N2O5 reactivity on ambient aerosol particles, Geophys. Res. Lett., 36, 10.1029/2009gl040248, 2009b.

Brown, S., Stark, H., Ciciora, S., McLaughlin, R., and Ravishankara, A. R.: Simultaneous in situ Detection of Atmospheric NO3 and N2O5 via Cavity Ring-down Spectroscopy, Rev. Sci. Instrum., 73, 3291-3301, 10.1063/1.1499214, 2002.

Brown, S. S., Ryerson, T. B., Wollny, A. G., Brock, C. A., Peltier, R., Sullivan, A. P., Weber, R. J., Dube, W. P., Trainer, M., Meagher, J. F., Fehsenfeld, F. C., and Ravishankara, A. R.: Variability in nocturnal nitrogen oxide processing and its role in regional air quality, Science, 311, 67-70, 10.1126/science.1120120, 2006.

Brown, S. S., Dube, W. P., Fuchs, H., Ryerson, T. B., Wollny, A. G., Brock, C. A., Bahreini, R., Middlebrook, A. M., Neuman, J. A., Atlas, E., Roberts, J. M., Osthoff, H. D., Trainer, M., Fehsenfeld, F. C., and Ravishankara, A. R.: Reactive uptake coefficients for N2O5 determined from aircraft measurements during the Second Texas Air Quality Study: Comparison to current model parameterizations, J. Geophys. Res.- Atmos., 114, D00F10(01-16), Artn D00f10
10.1029/2008jd011679, 2009.

Brown, S. S., and Stutz, J.: Nighttime radical observations and chemistry, Chem. Soc. Rev., 41, 6405-6447, 10.1039/c2cs35181a, 2012.

Brown, S. S., Dubé, W. P., Tham, Y. J., Zha, Q., Xue, L., Poon, S., Wang, Z., Blake, D. R., Tsui, W., Parrish, D. D., and Wang, T.: Nighttime chemistry at a high altitude site above Hong Kong, J. Geophys. Res.: Atmos., 121, 2457-2475, 10.1002/2015jd024566, 2016.

Chang, W. L., Bhave, P. V., Brown, S. S., Riemer, N., Stutz, J., and Dabdub, D.: Heterogeneous atmospheric chemistry, ambient measurements, and model calculations of N2O5: A review, Aerosol Sci. Technol., 45, 665-695, 2011.

Chen, X., Wang, H., Lu, K., Li, C., Zhai, T., Tan, Z., Ma, X., Yang, X., Liu, Y., Chen, S., Dong, H., Li, X., Wu, Z., Hu, M., Zeng, L., and Zhang, Y.: Field Determination of Nitrate Formation Pathway in Winter Beijing, Environmental Science & Technology, 54, 9243-9253, 10.1021/acs.est.0c00972, 2020.

Chen, X., Wang, H., and Lu, K.: Interpretation of NO 3–N 2 O 5 observation via steady state in high aerosol air mass: The impact of equilibrium coefficient in ambient conditions, Atmospheric Chemistry and Physics Discussions, 1-14, 2021.

Cosman, L. M., Knopf, D. A., and Bertram, A. K.: N2O5 reactive uptake on aqueous sulfuric acid solutions

coated with branched and straight-chain insoluble organic surfactants, J. Phys. Chem. A, 112, 2386-2396, 10.1021/jp710685r, 2008.
Danckwerts, P. V.: Continuous flow systems: distribution of residence times, Chem. Eng. Sci., 2, 1-13, 1953.
Davis, J. M., Bhave, P. V., and Foley, K. M.: Parameterization of N2O5 reaction probabilities on the surface of particles containing ammonium, sulfate, and nitrate, Atmos. Chem. Phys., 8, 5295-5311, 10.5194/acp-8-5295-2008, 2008.
Dentener, F. J., and Crutzen, P. J.: Reaction Of N2O5 On Tropospheric Aerosols - Impact On The Global Distributions Of NOx, O3, And OH, Journal of Geophysical Research Atmospheres, 98, 7149-7163, 1993.
Escoreia, E. N., Sjostedt, S. J., and Abbatt, J. P. D.: Kinetics of N2O5 Hydrolysis on Secondary Organic Aerosol and Mixed Ammonium Bisulfate-Secondary Organic Aerosol Particles, J. Phys. Chem. A, 114, 13113-13121, 10.1021/jp107721v, 2010.
Evans, M., and Jacob, D. J.: Impact of new laboratory studies of N2O5 hydrolysis on global model budgets of tropospheric nitrogen oxides, ozone, and OH, Geophys. Res. Lett., 32, 2005.
Folkers, M., Mentel, T. F., and Wahner, A.: Influence of an organic coating on the reactivity of aqueous aerosols probed by the heterogeneous hydrolysis of N2O5, Geophys. Res. Lett., 30, Artn 1644 10.1029/2003gl017168, 2003.
Fried, A., Henry, B. E., Calvert, J. G., and Mozurkewich, M.: THE REACTION PROBABILITY OF N_2O_5 WITH SULFURIC-ACID AEROSOLS AT STRATOSPHERIC TEMPERATURES AND COMPOSITIONS, J. Geophys. Res.- Atmos., 99, 3517-3532, 10.1029/93jd01907, 1994.
Fu, X., Wang, T., Gao, J., Wang, P., Liu, Y., Wang, S., Zhao, B., and Xue, L.: Persistent Heavy Winter Nitrate Pollution Driven by Increased Photochemical Oxidants in Northern China, Environ. Sci. Technol., 54, 3881-3889, 10.1021/acs.est.9b07248, 2020.
Fuchs, N. A., and Sutugin, A. G.: Highly Dispersed Aerosol, Halsted Press, 1970.
Gaston, C. J., Thornton, J. A., and Ng, N. L.: Reactive uptake of N2O5 to internally mixed inorganic and organic particles: the role of organic carbon oxidation state and inferred organic phase separations, Atmos. Chem. Phys., 14, 5693-5707, 10.5194/acp-14-5693-2014, 2014.
Gaston, C. J., and Thornton, J. A.: Reacto-Diffusive Length of N2O5 in Aqueous Sulfate- and Chloride-Containing Aerosol Particles, J. Phys. Chem. A, 120, 1039-1045, 10.1021/acs.jpca.5b11914, 2016.
Griffiths, P. T., Badger, C. L., Cox, R. A., Folkers, M., Henk, H. H., and Mentel, T. F.: Reactive Uptake of N2O5 by Aerosols Containing Dicarboxylic Acids. Effect of Particle Phase, Composition, and Nitrate Content, J. Phys. Chem. A, 113, 5082-5090, 10.1021/jp8096814, 2009.
Gross, S., Iannone, R., Xiao, S., and Bertram, A. K.: Reactive uptake studies of NO3 and N2O5 on alkenoic acid, alkanoate, and polyalcohol substrates to probe nighttime aerosol chemistry, PCCP, 11, 7792-7803, 10.1039/b904741g, 2009.
Hallquist, M., Stewart, D. J., Baker, J., and Cox, R. A.: Hydrolysis of N_2O_5 on submicron sulfuric acid aerosols, J. Phys. Chem. A, 104, 3984-3990, 10.1021/jp9939625, 2000.
Hallquist, M., Stewart, D. J., Stephenson, S. K., and Anthony Cox, R.: Hydrolysis of N_2O_5 on sub-micron sulfate aerosols, PCCP, 5, 3453, 10.1039/b301827j, 2003.
Hu, J. H., and Abbatt, J. P. D.: Reaction probabilities for N2O5 hydrolysis on sulfuric acid and ammonium sulfate aerosols at room temperature, J. Phys. Chem. A, 101, 871-878, DOI 10.1021/jp9627436, 1997.
Huang, Y., Coggon, M., Zhao, R., Lignell, H., Bauer, M., Flagan, R., and Seinfeld, J.: The Caltech Photooxidation Flow Tube reactor: Design, fluid dynamics and characterization, Atmospheric Measurement Techniques, 10, 839-867, 10.5194/amt-10-839-2017, 2017.

Kane, S. M., Caloz, F., and Leu, M. T.: Heterogeneous uptake of gaseous N_2O_5 by $(NH_4)_2SO_4$, NH_4HSO_4, and H_2SO_4 aerosols, J. Phys. Chem. A, 105, 6465-6470, 10.1021/jp010490x, 2001.

Karagulian, F., Santschi, C., and Rossi, M.: The heterogeneous chemical kinetics of N 2 O 5 on CaCO 3 and other atmospheric mineral dust surrogates, Atmos. Chem. Phys., 6, 1373-1388, 2006.

Lambe, A., Ahern, A., Williams, L., Slowik, J., Wong, J., Abbatt, J., Brune, W., Ng, N., Wright, J., and Croasdale, D.: Characterization of aerosol photooxidation flow reactors: heterogeneous oxidation, secondary organic aerosol formation and cloud condensation nuclei activity measurements, Atmospheric Measurement Techniques, 4, 445-461, 2011.

Li, C. M., Wang, H. C., Chen, X. R., Zhai, T. Y., Chen, S. Y., Li, X., Zeng, L. M., and Lu, K. D.: Thermal dissociation cavity-enhanced absorption spectrometer for measuring NO2, RO2NO2, and RONO2 in the atmosphere, Atmospheric Measurement Techniques, 14, 4033-4051, 10.5194/amt-14-4033-2021, 2021.

Li, Q., Zhang, L., Wang, T., Tham, Y. J., Ahmadov, R., Xue, L., Zhang, Q., and Zheng, J.: Impacts of heterogeneous uptake of dinitrogen pentoxide and chlorine activation on ozone and reactive nitrogen partitioning: improvement and application of the WRF-Chem model in southern China, Atmos. Chem. Phys., 16, 14875-14890, 10.5194/acp-16-14875-2016, 2016.

Liu, X., Gu, J., Li, Y., Cheng, Y., Qu, Y., Han, T., Wang, J., Tian, H., Chen, J., and Zhang, Y.: Increase of aerosol scattering by hygroscopic growth: Observation, modeling, and implications on visibility, Atmos. Res. , 132, 91-101, 2013.

Lowe, D., Archer-Nicholls, S., Morgan, W., Allan, J., Utembe, S., Ouyang, B., Aruffo, E., Le Breton, M., Zaveri, R. A., and Di Carlo, P.: WRF-Chem model predictions of the regional impacts of N 2 O 5 heterogeneous processes on night-time chemistry over north-western Europe, Atmos. Chem. Phys., 15, 1385-1409, 2015.

Macintyre, H., and Evans, M.: Sensitivity of a global model to the uptake of N 2 O 5 by tropospheric aerosol, Atmos. Chem. Phys., 10, 7409-7414, 2010.

Martin, S. T.: Phase transitions of aqueous atmospheric particles, Chem. Rev., 100, 3403-3454, 2000.

McDuffie, E. E., Fibiger, D. L., Dubé, W. P., Lopez-Hilfiker, F., Lee, B. H., Thornton, J. A., Shah, V., Jaeglé, L., Guo, H., Weber, R. J., Michael Reeves, J., Weinheimer, A. J., Schroder, J. C., Campuzano-Jost, P., Jimenez, J. L., Dibb, J. E., Veres, P., Ebben, C., Sparks, T. L., Wooldridge, P. J., Cohen, R. C., Hornbrook, R. S., Apel, E. C., Campos, T., Hall, S. R., Ullmann, K., and Brown, S. S.: Heterogeneous N_2O_5 Uptake During Winter: Aircraft Measurements During the 2015 WINTER Campaign and Critical Evaluation of Current Parameterizations, J. Geophys. Res.: Atmos., 123, 4345-4372, 10.1002/2018jd028336, 2018.

McDuffie, E. E., Womack, C. C., Fibiger, D. L., Dube, W. P., Franchin, A., Middlebrook, A. M., Goldberger, L., Lee, B. H., Thornton, J. A., Moravek, A., Murphy, J. G., Baasandorj, M., and Brown, S. S.: On the contribution of nocturnal heterogeneous reactive nitrogen chemistry to particulate matter formation during wintertime pollution events in Northern Utah, Atmos. Chem. Phys., 19, 9287-9308, 10.5194/acp-19-9287-2019, 2019.

McNeill, V. F., Patterson, J., Wolfe, G. M., and Thornton, J. A.: The effect of varying levels of surfactant on the reactive uptake of N2O5 to aqueous aerosol, Atmos. Chem. Phys., 6, 1635-1644, 10.5194/acp-6-1635-2006, 2006.

Mentel, T. F., Sohn, M., and Wahner, A.: Nitrate effect in the heterogeneous hydrolysis of dinitrogen pentoxide on aqueous aerosols, PCCP, 1, 5451-5457, 10.1039/a905338g, 1999.

Mielke, L. H., Stutz, J., Tsai, C., Hurlock, S. C., Roberts, J. M., Veres, P. R., Froyd, K. D., Hayes, P. L., Cubison, M. J., Jimenez, J. L., Washenfelder, R. A., Young, C. J., Gilman, J. B., de Gouw, J. A., Flynn, J. H., Grossberg, N., Lefer, B. L., Liu, J., Weber, R. J., and Osthoff, H. D.: Heterogeneous formation of nitryl chloride and its role as a nocturnal NOx reservoir species during CalNex-LA 2010, J. Geophys. Res.: Atmos., 118, 10,638-610,652, 10.1002/jgrd.50783, 2013.

Mitroo, D., Gill, T. E., Haas, S., Pratt, K. A., and Gaston, C. J.: CINO2 Production from N2O5 Uptake on Saline Playa Dusts: New Insights into Potential Inland Sources of CINO2, Environmental Science & Technology, 53, 7442-7452, 10.1021/acs.est.9b01112, 2019.

Mozurkewich, M., and Calvert, J. G.: REACTION PROBABILITY OF N2O5 ON AQUEOUS AEROSOLS, J. Geophys. Res.- Atmos., 93, 15889-15896, 10.1029/JD093iD12p15889, 1988.

Murray, L. T., Fiore, A. M., Shindell, D. T., Naik, V., and Horowitz, L. W.: Large uncertainties in global hydroxyl projections tied to fate of reactive nitrogen and carbon, Proceedings of the National Academy of Sciences, 118, 2021.

Osthoff, H. D., Roberts, J. M., Ravishankara, A. R., Williams, E. J., Lerner, B. M., Sommariva, R., Bates, T. S., Coffman, D., Quinn, P. K., Dibb, J. E., Stark, H., Burkholder, J. B., Talukdar, R. K., Meagher, J., Fehsenfeld, F. C., and Brown, S. S.: High levels of nitryl chloride in the polluted subtropical marine boundary layer, Nat. Geosci. , 1, 324-328, 10.1038/ngeo177, 2008.

Phillips, G. J., Thieser, J., Tang, M., Sobanski, N., Schuster, G., Fachinger, J., Drewnick, F., Borrmann, S., Bingemer, H., Lelieveld, J., and Crowley, J. N.: Estimating N_2O_5 uptake coefficients using ambient measurements of NO_3, N_2O_5, $ClNO_2$ and particle-phase nitrate, Atmos. Chem. Phys., 16, 13231-13249, 10.5194/acp-16-13231-2016, 2016.

Platt, U. F., Winer, A. M., Biermann, H. W., Atkinson, R., and Pitts, J. N.: Measurement of nitrate radical concentrations in continental air, Environmental Science & Technology, 18, 365-369, 10.1021/es00123a015, 1984.

Prabhakar, G., Parworth, C. L., Zhang, X. L., Kim, H., Young, D. E., Beyersdorf, A. J., Ziemba, L. D., Nowak, J. B., Bertram, T. H., Faloona, I. C., Zhang, Q., and Cappa, C. D.: Observational assessment of the role of nocturnal residual-layer chemistry in determining daytime surface particulate nitrate concentrations, Atmos. Chem. Phys., 17, 14747-14770, 10.5194/acp-17-14747-2017, 2017.

Riedel, T. P., Bertram, T. H., Crisp, T. A., Williams, E. J., Lerner, B. M., Vlasenko, A., Li, S. M., Gilman, J., de Gouw, J., Bon, D. M., Wagner, N. L., Brown, S. S., and Thornton, J. A.: Nitryl Chloride and Molecular Chlorine in the Coastal Marine Boundary Layer, Environmental Science & Technology, 46, 10463-10470, 10.1021/es204632r, 2012a.

Riedel, T. P., Bertram, T. H., Ryder, O. S., Liu, S., Day, D. A., Russell, L. M., Gaston, C. J., Prather, K. A., and Thornton, J. A.: Direct N_2O_5 reactivity measurements at a polluted coastal site, Atmos. Chem. Phys., 12, 2959-2968, 10.5194/acp-12-2959-2012, 2012b.

Riedel, T. P., Wagner, N. L., Dube, W. P., Middlebrook, A. M., Young, C. J., Ozturk, F., Bahreini, R., VandenBoer, T. C., Wolfe, D. E., Williams, E. J., Roberts, J. M., Brown, S. S., and Thornton, J. A.: Chlorine activation within urban or power plant plumes: Vertically resolved ClNO2 and Cl-2 measurements from a tall tower in a polluted continental setting, J. Geophys. Res.- Atmos., 118, 8702-8715, 10.1002/jgrd.50637, 2013.

Riemer, N., Vogel, H., Vogel, B., Schell, B., Ackermann, I., Kessler, C., and Hass, H.: Impact of the heterogeneous hydrolysis of N2O5 on chemistry and nitrate aerosol formation in the lower troposphere under photosmog conditions, J. Geophys. Res.- Atmos., 108, 10.1029/2002jd002436, 2003.

Riemer, N., Vogel, H., Vogel, B., Anttila, T., Kiendler-Scharr, A., and Mentel, T. F.: Relative importance of organic coatings for the heterogeneous hydrolysis of N2O5during summer in Europe, J. Geophys. Res. , 114, 10.1029/2008jd011369, 2009.

Royer, H. M., Mitroo, D., Hayes, S. M., Haas, S. M., Pratt, K. A., Blackwelder, P. L., Gill, T. E., and Gaston, C. J.: The Role of Hydrates, Competing Chemical Constituents, and Surface Composition on CINO2 Formation, Environmental Science & Technology, 55, 2869-2877, 10.1021/acs.est.0c06067, 2021.

Sarwar, G., Simon, H., Bhave, P., and Yarwood, G.: Examining the impact of heterogeneous nitryl chloride production on air quality across the United States, Atmospheric Chemistry & Physics, 12, 6455-6473, 10.5194/acp-12-6455-2012, 2012.

Schweitzer, F., Mirabel, P., and George, C.: Multiphase chemistry of N2O5, ClNO2, and BrNO2, The Journal of Physical Chemistry A, 102, 3942-3952, 1998.

Tang, M., Telford, P., Pope, F. D., Rkiouak, L., Abraham, N., Archibald, A. T., Braesicke, P., Pyle, J., McGregor, J., and Watson, I.: Heterogeneous reaction of N 2 O 5 with airborne TiO 2 particles and its implication for stratospheric particle injection, Atmos. Chem. Phys., 14, 6035-6048, 2014.

Tham, Y. J., Wang, Z., Li, Q. Y., Yun, H., Wang, W. H., Wang, X. F., Xue, L. K., Lu, K. D., Ma, N., Bohn, B., Li, X., Kecorius, S., Gross, J., Shao, M., Wiedensohler, A., Zhang, Y. H., and Wang, T.: Significant concentrations of nitryl chloride sustained in the morning: investigations of the causes and impacts on ozone production in a polluted region of northern China, Atmos. Chem. Phys., 16, 14959-14977, 10.5194/acp-16-14959-2016, 2016.

Tham, Y. J., Wang, Z., Li, Q. Y., Wang, W. H., Wang, X. F., Lu, K. D., Ma, N., Yan, C., Kecorius, S., Wiedensohler, A., Zhang, Y. H., and Wang, T.: Heterogeneous N2O5 uptake coefficient and production yield of ClNO2 in polluted northern China: roles of aerosol water content and chemical composition, Atmos. Chem. Phys., 18, 13155-13171, 10.5194/acp-18-13155-2018, 2018.

Thornton, J. A., Braban, C. F., and Abbatt, J. P. D.: N2O5 hydrolysis on sub-micron organic aerosols: the effect of relative humidity, particle phase, and particle size, PCCP, 5, 4593, 10.1039/b307498f, 2003.

Thornton, J. A., and Abbatt, J. P. D.: N2O5 reaction on submicron sea salt aerosol: Kinetics, products, and the effect of surface active organics, J. Phys. Chem. A, 109, 10004-10012, 10.1021/jp054183t, 2005.

Thornton, J. A., Kercher, J. P., Riedel, T. P., Wagner, N. L., Cozic, J., Holloway, J. S., Dube, W. P., Wolfe, G. M., Quinn, P. K., Middlebrook, A. M., Alexander, B., and Brown, S. S.: A large atomic chlorine source inferred from mid-continental reactive nitrogen chemistry, Nature, 464, 271-274, 10.1038/nature08905, 2010.

Van Doren, J. M., Watson, L. R., Davidovits, P., Worsnop, D. R., Zahniser, M. S., and Kolb, C. E.: Temperature dependence of the uptake coefficients of nitric acid, hydrochloric acid and nitrogen oxide (N2O5) by water droplets, J. Phys. Chem., 94, 3265-3269, 1990.

Wagner, N. L., Riedel, T. P., Young, C. J., Bahreini, R., Brock, C. A., Dubé, W. P., Kim, S., Middlebrook, A. M., Öztürk, F., Roberts, J. M., Russo, R., Sive, B., Swarthout, R., Thornton, J. A., VandenBoer, T. C., Zhou, Y., and Brown, S. S.: N2O5 uptake coefficients and nocturnal NO2 removal rates determined from ambient wintertime measurements, J. Geophys. Res.: Atmos., 118, 9331-9350, 10.1002/jgrd.50653, 2013.

Wahner, A., Mentel, T. F., Sohn, M., and Stier, J.: Heterogeneous reaction of N2O5 on sodium nitrate aerosol, J. Geophys. Res.: Atmos., 103, 31103-31112, 10.1029/1998jd100022, 1998.

Wang, H., Chen, J., and Lu, K.: Development of a portable cavity-enhanced absorption spectrometer for the measurement of ambient NO₃ and N₂O₅: experimental setup, lab characterizations, and field applications in a polluted urban environment, Atmospheric Measurement Techniques, 10, 1465-1479, 10.5194/amt-10-1465-2017, 2017a.

Wang, H., Lu, K., Chen, X., Zhu, Q., Chen, Q., Guo, S., Jiang, M., Li, X., Shang, D., Tan, Z., Wu, Y., Wu, Z., Zou, Q., Zheng, Y., Zeng, L., Zhu, T., Hu, M., and Zhang, Y.: High N_2O_5 Concentrations Observed in Urban Beijing: Implications of a Large Nitrate Formation Pathway, Environ Sci Tech Let, 4, 416-420, 10.1021/acs.estlett.7b00341, 2017b.

Wang, H., Chen, X., Lu, K., Tan, Z., Ma, X., Wu, Z., Li, X., Liu, Y., Shang, D., Wu, Y., Zeng, L., Hu, M., Schmitt, S., Kiendler-Scharr, A., Wahner, A., and Zhang, Y.: Wintertime N2O5 uptake coefficients over the North China

971 Plain, Science Bulletin, 65, 765-774, https://doi.org/10.1016/j.scib.2020.02.006, 2020a.
972 Wang, H. C., Lu, K. D., Chen, X. R., Zhu, Q. D., Chen, Q., Guo, S., Jiang, M. Q., Li, X., Shang, D. J., Tan, Z. F.,
973 Wu, Y. S., Wu, Z. J., Zou, Q., Zheng, Y., Zeng, L. M., Zhu, T., Hu, M., and Zhang, Y. H.: High N2O5
974 Concentrations Observed in Urban Beijing: Implications of a Large Nitrate Formation Pathway, Environ Sci Tech
975 Let, 4, 416-420, 10.1021/acs.estlett.7b00341, 2017c.
976 Wang, H. C., Lu, K. D., Chen, X. R., Zhu, Q. D., Wu, Z. J., Wu, Y. S., and Sun, K.: Fast particulate nitrate
977 formation via N2O5 uptake aloft in winter in Beijing, Atmos. Chem. Phys., 18, 10483-10495, 10.5194/acp-18-
978 10483-2018, 2018a.
979 Wang, H. C., Lu, K. D., Guo, S., Wu, Z. J., Shang, D. J., Tan, Z. F., Wang, Y. J., Le Breton, M., Lou, S. R., Tang,
980 M. J., Wu, Y. S., Zhu, W. F., Zheng, J., Zeng, L. M., Hallquist, M., Hu, M., and Zhang, Y. H.: Efficient N2O5
981 uptake and NO3 oxidation in the outflow of urban Beijing, Atmos. Chem. Phys., 18, 9705-9721, 10.5194/acp-
982 18-9705-2018, 2018b.
983 Wang, H. C., Chen, X. R., Lu, K. D., Hu, R. Z., Li, Z. Y., Wang, H. L., Ma, X. F., Yang, X. P., Chen, S. Y., Dong,
984 H. B., Liu, Y., Fang, X., Zeng, L. M., Hu, M., and Zhang, Y. H.: NO3 and N2O5 chemistry at a suburban site
985 during the EXPLORE-YRD campaign in 2018, Atmos. Environ., 224, ARTN 117180
986 10.1016/j.atmosenv.2019.117180, 2020b.
987 Wang, H. C., Peng, C., Wang, X., Lou, S. R., Lu, K. D., Gan, G. C., Jia, X. H., Chen, X. R., Chen, J., Wang, H.
988 L., Fan, S. J., Wang, X. M., and Tang, M. J.: N2O5 uptake onto saline mineral dust: a potential missing source of
989 tropospheric ClNO2 in inland China, Atmos. Chem. Phys., 22, 1845-1859, 10.5194/acp-22-1845-2022, 2022.
990 Wang, W., Wang, Z., Yu, C., Xia, M., Peng, X., Zhou, Y., Yue, D., Ou, Y., and Wang, T.: An in situ flow tube
991 system for direct measurement of N2O5 heterogeneous uptake coefficients in polluted environments,
992 Atmospheric Measurement Techniques, 11, 5643-5655, 10.5194/amt-11-5643-2018, 2018c.
993 Wang, X., Wang, H., Xue, L., Wang, T., Wang, L., Gu, R., Wang, W., Tham, Y. J., Wang, Z., Yang, L., Chen, J.,
994 and Wang, W.: Observations of N_2O_5 and $ClNO_2$ at a polluted urban surface site in North China: High N_2O_5
995 uptake coefficients and low $ClNO_2$ product yields, Atmos. Environ., 156, 125-134,
996 10.1016/j.atmosenv.2017.02.035, 2017d.
997 Wang, Y. L., Song, W., Yang, W., Sun, X. C., Tong, Y. D., Wang, X. M., Liu, C. Q., Bai, Z. P., and Liu, X. Y.:
998 Influences of atmospheric pollution on the contributions of major oxidation pathways to PM2. 5 nitrate formation
999 in Beijing, J. Geophys. Res.: Atmos., 124, 4174-4185, 2019.
1000 Wang, Z., Wang, W., Tham, Y. J., Li, Q., Wang, H., Wen, L., Wang, X., and Wang, T.: Fast heterogeneous N2O5
1001 uptake and ClNO2 production in power plant and industrial plumes observed in the nocturnal residual layer over
1002 the North China Plain, Atmos. Chem. Phys., 17, 12361-12378, 10.5194/acp-17-12361-2017, 2017e.
1003 Wang, Z., Wang, W. H., Tham, Y. J., Li, Q. Y., Wang, H., Wen, L., Wang, X. F., and Wang, T.: Fast heterogeneous
1004 N2O5 uptake and ClNO2 production in power plant and industrial plumes observed in the nocturnal residual
1005 layer over the North China Plain, Atmos. Chem. Phys., 17, 12361-12378, 10.5194/acp-17-12361-2017, 2017f.
1006 Wu, C., Zhang, S., Wang, G., Lv, S., Li, D., Liu, L., Li, J., Liu, S., Du, W., and Meng, J.: Efficient heterogeneous
1007 formation of ammonium nitrate on the saline mineral particle surface in the atmosphere of East Asia during dust
1008 storm periods, Environmental Science & Technology, 54, 15622-15630, 2020.
1009 Xia, M., Wang, W., Wang, Z., Gao, J., Li, H., Liang, Y., Yu, C., Zhang, Y., Wang, P., Zhang, Y., Bi, F., Cheng, X.,
1010 and Tao, W.: Heterogeneous Uptake of N2O5 in Sand Dust and Urban Aerosols Observed during the Dry Season
1011 in Beijing, Atmosphere, 10, 204, 10.3390/atmos10040204, 2019.
1012 Yu, C., Wang, Z., Xia, M., Fu, X., Wang, W., Yee Jun, T., Chen, T., Zheng, P., Li, H., Shan, Y., Wang, X., Xue,
1013 L., Zhou, Y., Yue, D., Ou, Y., Gao, J., Lu, K., Brown, S., Zhang, Y., and Tao, W.: Heterogeneous N_2O_5 reactions

on atmospheric aerosols at four Chinese sites: improving model representation of uptake parameters, Atmos. Chem. Phys., 20, 4367-4378, 10.5194/acp-20-4367-2020, 2020a.

Yu, C., Wang, Z., Xia, M., Fu, X., Wang, W. H., Tham, Y. J., Chen, T. S., Zheng, P. G., Li, H. Y., Shan, Y., Wang, X. F., Xue, L. K., Zhou, Y., Yue, D. L., Ou, Y. B., Gao, J., Lu, K. D., Brown, S. S., Zhang, Y. H., and Wang, T.: Heterogeneous N2O5 reactions on atmospheric aerosols at four Chinese sites: improving model representation of uptake parameters, Atmos. Chem. Phys., 20, 4367-4378, 10.5194/acp-20-4367-2020, 2020b.

Yun, H., Wang, T., Wang, W. H., Tham, Y. J., Li, Q. Y., Wang, Z., and Poon, S. C. N.: Nighttime NOx loss and ClNO2 formation in the residual layer of a polluted region: Insights from field measurements and an iterative box model, Sci. Total Environ., 622, 727-734, 10.1016/j.scitotenv.2017.11.352, 2018.